Published by Institute of Physics Publishing for SISSA

Received: *January 16, 2007*
Accepted: *February 13, 2008*
Published: *February 21, 2008*

Heavy quark diffusion in QCD and $\mathcal{N}=4$ SYM at next-to-leading order

Simon Caron-Huot and Guy D. Moore

McGill University Dept. of Physics,
3600 rue University, Montréal QC H3A 2T8 Canada
E-mail: scaronhuot@physics.mcgill.ca, guymoore@physics.mcgill.ca

Abstract: We present the full details of a calculation at next-to-leading order of the momentum diffusion coefficient of a heavy quark in a hot, weakly coupled, QCD plasma. Corrections arise at $\mathcal{O}(g_{\rm s})$; physically they represent interference between overlapping scatterings, as well as soft, electric scale ($p \sim gT$) gauge field physics, which we treat using the hard thermal loop (HTL) effective theory. In 3-color, 3-flavor QCD, the momentum diffusion constant of a fundamental representation heavy quark at NLO is $\kappa = \frac{16\pi}{3}\alpha_{\rm s}^2 T^3(\ln\frac{1}{g_{\rm s}} + 0.07428 + 1.9026 g_{\rm s})$. We extend the computation to a heavy fundamental representation "probe" quark in large $N_{\rm c}$, $\mathcal{N}=4$ Super Yang-Mills theory, where the result is $\kappa^{(SYM)} = \frac{\lambda^2 T^3}{6\pi}\left(\ln\frac{1}{\sqrt{\lambda}} + 0.4304 + 0.8010\sqrt{\lambda}\right)$ (where $\lambda = g^2 N_{\rm c}$ is the t'Hooft coupling). In the absence of some resummation technique, the convergence of perturbation theory is poor.

Keywords: Thermal Field Theory, Quantum Dissipative Systems, NLO Computations, QCD.

JHEP02(2008)081

Contents

1. Introduction **1**

2. Overview and results **3**
- 2.1 Definition of heavy quark diffusion 3
- 2.2 Qualitative origin of NLO effects 3
- 2.3 Results: QCD 5
- 2.4 $\mathcal{N}$=4 super Yang-Mills 8

3. Effective theory and leading-order analysis **10**

4. Details of the calculation **12**
- 4.1 Formalism and diagrams 12
- 4.2 Real part of self-energy diagrams (A) and (C) 15
- 4.3 Self-energy (A): imaginary part 16
  - 4.3.1 Overview of the calculation 16
  - 4.3.2 Evaluation of the cuts 17
  - 4.3.3 The Lorentz structure 21
  - 4.3.4 Final expressions for diagram (A) 23
  - 4.3.5 A subtlelty near $q^0 = q_\perp$ 26
- 4.4 The diagram (B) 27
- 4.5 Self-energy (C): imaginary part 30
- 4.6 The diagram (D) 32

5. $\mathcal{N}$=4 super Yang-Mills **32**

A. The functions $M^{00}(Q,R)$ and $L(Q)$ **36**

1. Introduction

In the earliest stages of the Big Bang the universe was a relativistic plasma. We can now produce such a relativistic plasma in the lab via heavy ion collisions. In both cases the plasma is transient-in the early universe it lasted only around 10^{-6} seconds and in a heavy ion collision it lasts little more than 10^{-23} seconds. Since a system which remains always in equilibrium leaves essentially no traces of its earlier state, the most interesting physics in both situations is nonequilibrium physics. And in the early universe at temperatures above 10's of GeV [relevant for electroweak baryogenesis [1], leptogenesis [2], gravitino production [3], moduli production and destruction, and other relics] that plasma was weakly

JHEP02(2008)081

coupled. The same is true in principle for the early development of extremely high energy heavy ion collisions, though it is an open question whether this is a reasonable treatment at available energies.

The natural language to study such plasmas is nonequilibrium quantum field theory. For plasmas near equilibrium (relevant for most of these interesting problems) one can study linear deviations from (local) equilibrium by studying unequal-time equilibrium correlations and using linear response theory [4]. The tools for defining equilibrium finite temperature field theory and for performing weak coupling expansions have been known for over 40 years [5, 6]. Nevertheless, our ability to calculate thermal and nonequilibrium phenomena is surprisingly immature. For thermodynamical properties we now understand how to compute perturbatively very well; for instance, the best known quantity, the thermodynamic pressure, is known past fifth order [7 – 9]. We also understand that to compute real-time processes we need to perform a resummation of certain plasma effects via the so-called Hard Thermal Loops (HTL's) [10].

However surprisingly few gauge invariant real-time correlation functions have been computed even at leading order, and even fewer are known beyond this level. In particular, transport coefficients — shear viscosity, baryon number diffusion, electrical conductivity, heavy quark diffusion, bulk viscosity, and so on — are of considerable importance, since they describe the relaxation of a system which is relatively close to equilibrium. However, even leading order calculations of these quantities only became available quite recently, and *none* of them are known beyond leading order.

This is a major gap in our understanding of finite temperature field theory. In particular, it has been known for some time that the rate of convergence of the perturbative series in the thermal theory can be much worse than in the vacuum theory. For instance, Braaten and Nieto [8] argued that the convergence of perturbation theory was poor unless $\alpha_{\rm s} \lesssim 0.1$, due to physics at the so-called electric screening scale $\sim gT$ (where the loop expansion really is only an expansion into powers of g.) It may be possible to rescue, or at least improve, the convergence of perturbation theory using various resummation techniques [11, 12]. However neither of these issues has been explored for dynamical (unequal time) quantities. In this context exactly one interesting gauge invariant quantity is known at next-to-leading order; the deeply virtual dilepton production rate [13]. However this quantity involves short physical time scales and is not sensitive to the electric gT scale, and is therefore not representative of the other transport coefficients, which are. For these "soft-sensitive" quantities, we do not know what a next-to-leading order computation involves, we do not know how well the series will converge, and we do not know what resummation techniques might be available or how well they may work.

The simplest such quantity is the heavy quark diffusion coefficient, first computed at leading order in [14]. This is a quantity of phenomenological interest, which sets the rate at which the velocity of a heavy quark equilibrates with that of its environment. In a recent Letter [15] we have presented the result of a computation of the heavy quark diffusion coefficient in full QCD to next-to-leading order. Here we present the full details of this calculation, as well as its extension to $\mathcal{N}$=4 super-Yang-Mills theory ($\mathcal{N}$=4 SYM). An outline of the paper is as follows. In the next section we summarize the problem, discuss

JHEP02(2008)081

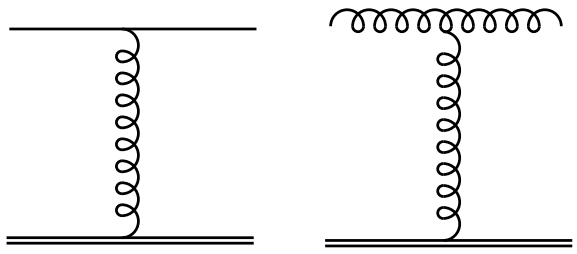

Figure 1: Processes responsible for heavy quark diffusion at leading order: Coulombic scattering between a heavy quark (double line) and either a quark or a gluon.

the relevant physics, and present the results. Then section 3 presents our approach (HTL effective field theory) and reviews the leading order calculation. Section 4 presents the body of the calculation of the NLO diffusion coefficient, and section 5 extends this treatment to $\mathcal{N}$=4 Super-Yang-Mills theory. A technical appendix discusses the analytical properties of some of the functions we encounter in the calculation.

2. Overview and results

2.1 Definition of heavy quark diffusion

A heavy quark, $M \gg T$, in or near equilibrium has a typical momentum squared $\mathbf{p}^2 \sim MT \gg T^2$ large compared to the plasma scale and it therefore takes a parametrically long time for the momentum to change appreciably. This means that momentum changes accumulate from many uncorrelated "kicks," so on long time scales p will evolve via Langevin dynamics,

$$\frac{dp_i}{dt} = -\eta_D\, p_i + \xi_i(t)\,, \quad \langle \xi_i(t)\xi_j(t')\rangle = \kappa\,\delta_{ij}\delta(t-t')\,. \tag{2.1}$$

The relaxation rate η_D and the momentum diffusion coefficient κ are related by a fluctuation-dissipation relation, $\eta_D = \frac{\kappa}{2MT}$, which follows on general thermodynamical grounds. Thus the dynamics of the nonrelativistic heavy quark is completely set by the single parameter κ, which we compute to next-to-leading order.

2.2 Qualitative origin of NLO effects

At leading order in the weak coupling expansion, the momentum diffusion coefficient is set by the t-channel Coulomb scattering processes illustrated in figure 1, in which the scattering target can be a light quark or a gluon (Compton-like processes are suppressed for nonrelativistic heavy quarks.) An important feature of weakly coupled plasmas, relativistic and nonrelativistic, is that the total rate for Coulomb scattering is quadratically divergent in the limit of small momentum transfer $|\mathbf{q}|$ [16]. Such a divergence is of course unphysical in a medium of charged particles, and is cut off by screening effects[1] at the momentum scale $q \sim m_D \sim gT$.

[1] In relativistic plasmas there still remains a logarithmic divergence due to un-screened magnetic scatterings, but this cancels in physical quantities and will not concern us here.

JHEP02(2008)081

The momentum diffusion coefficient κ is sensitive not to the total scattering rate, but to the weighted average,

$$\kappa \equiv \frac{1}{3} \int d^3q \frac{d\Gamma(q)}{d^3q} q^2 \,, \tag{2.2}$$

where $d\Gamma(q)/d^3q$ denotes the differential probability per unit time for the momentum of the heavy quark to change by $\mathbf{q}$. The two additional powers of q^2 present in eq. (2.2) reduce the quadratic divergence of the total rate $\int d^3q d\Gamma/d^3q$ to a logarithmic divergence, cut off at $q \sim m_D$. The logarithm reflects the fact that the heavy quark momentum diffuses due to a range of momentum transfers, from the many soft scattering events, which individually have $q \sim gT$ but occur on a rate $\Gamma_{\rm soft} \sim g^2 T$, to the rare hard scattering events with $q \sim T$, occurring on a rate $\Gamma_{\rm hard} \sim g^4 T$.

Usually interaction corrections involve powers of g^2, and for large momentum transfer processes this is true. But the presence of the Coulombic divergence, cut off by screening effects, means that the details of soft momentum exchange and plasma screening are relevant to heavy quark diffusion already at leading order. Now consider the contribution from gluons to the Debye screening scale [17]:

$$m_D^2 = 4 T_A \, g^2 \int \frac{d^3k}{(2\pi)^3} \frac{n_B(k)}{k} + (\text{fermion contribution}) \,. \tag{2.3}$$

Here $T_A = N_{\rm c} = 3$ is the trace normalization of the adjoint representation and n_B is the Bose distribution function. At small k the integral behaves like $\sim g^2 T \int d|k|$, due to the singular nature of the Bose-Einstein function $n_B(k) \sim T/k$. Thus the contribution from gluons with $k \sim gT$ represents $\mathcal{O}(g)$ of the total strength of plasma screening.

However, the soft gluon contribution is not computed correctly by the above expression. The derivation of eq. (2.3) assumed free massless propagation of the particles responsible for screening, but gluons with $\mathcal{O}(gT)$ momenta themselves experience $\mathcal{O}(1)$ screening effects. Therefore one must recompute that part of plasma screening which arises from the $\mathcal{O}(gT)$ gluons. This calculation is complicated by the fact that interactions between soft gluons are also strongly modified by plasma effects, described by the HTL effective theory [10, 18]. Thus, since a relative $\mathcal{O}(g)$ fraction of eq. (2.3) arises from soft gluons, a correct treatment of the effect they produce will produce an $\mathcal{O}(g)$ correction to the physics which cuts off the infrared logarithm in κ, and therefore an $\mathcal{O}(g)$ correction to the result.

For similar reasons, in an $\mathcal{O}(g)$ fraction of soft scattering events, the plasma particle which strikes the heavy quark is itself a soft gluon with momentum $\sim gT$. But the dispersion and spectral weight of such gluons are strongly modified by the plasma and this contribution to the "target density" must also be reconsidered.

Other NLO corrections can be expected to arise from interference between overlapping scattering events, as illustrated in figure 2. Since the *total* scattering rate is $\sim g^2 T$, both for the heavy quark and for the light particles which scatter it, and since small angle scatterings can have a duration up to $\sim 1/gT$ (this can be read off, for instance, from the virtuality of the exchanged gluon), an $\mathcal{O}(g)$ fraction of scattering events overlap with another scattering. Thus the individual diagrams in figure 2 are only down by $\mathcal{O}(g)$ relative to the leading processes. Corresponding virtual corrections to the leading order scattering

JHEP02(2008)081

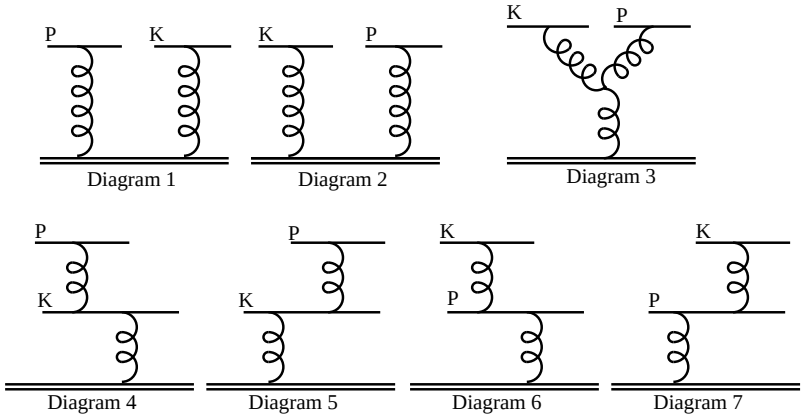

Figure 2: Diagrams which can interfere when two scattering processes overlap. Here K and P are the initial momenta of two distinct hard particles, which can be quarks or gluons.

process will naturally also arise at this order. However, the appropriate question to ask is not about the probability for scattering events to overlap, but rather how much do they interfere with each other. In QED, the small angle scattering of a particle occurring during another scattering event has little impact on that event, and correspondingly one finds a parametric cancellation between diagrams 1 and 2 of figure 2 (and between diagrams 4 and 5 and between diagrams 6 and 7, and among the associated virtual processes; diagram 3 is absent altogether in QED.) However, in QCD, instead of a cancellation one gets a commutator of group theory factors: the very frequent soft scatterings which occur in the plasma *do* matter, because they change the colors of the particles.

Note however that this source of $\mathcal{O}(g)$ NLO corrections and the preceding one are not clearly distinct. Indeed, diagram 3 of figure 2 can be understood as the special case of the diagram in figure 1, where the external gluons are soft and in the Landau cut. This suggests that, to make the qualitative discussion here more precise, we will need to perform a careful diagrammatic approach based on power counting. There is one common feature of the sources for correction we have listed, however; all involve the influence of soft gluons. This observation suggests that the calculation may be rephrased in terms of an effective theory of gT scale physics, in which the hard scale $\sim T$ has been integrated out. This is precisely Braaten and Pisarski's HTL effective theory [10]. Carrying out a careful diagrammatic calculation within this effective theory is the subject of the body of this paper; in the remainder of this section we will present the results.

2.3 Results: QCD

The squared matrix elements for the processes of figure 1, summed over the initial and final states of the light scattering targets and final states of the heavy quark, and averaged

over the initial states of the heavy quark, have been evaluated in [19], yielding

$$\kappa^{LO} \equiv \frac{g^4 C_H}{12\pi^3}\int_0^\infty k^2 dk \int_0^{2k} \frac{q^3 dq}{(q^2+m_D^2)^2} \times \left\{ \begin{array}{l} N_c\, n_B(k)(1{+}n_B(k)) \left(2-\frac{q^2}{k^2}+\frac{q^4}{4k^2}\right) \\ +N_f\, n_F(k)(1{-}n_F(k)) \left(2-\frac{q^2}{2k^2}\right), \end{array} \right. \tag{2.4}$$

where $C_H = \frac{4}{3}$ in QCD is the quadratic Casimir of the heavy quark representation, and $m_D = \sqrt{1.5}gT$ in QCD with $N_{\rm f}{=}3$ flavors of light quarks. Formally taking $m_D \ll T$, the integral is dominated by $k \sim T$ and q in the logarithmic range $m_D \lesssim q \lesssim T$. The leading behavior in g of eq. (2.4) can be obtained from the leading behavior in m_D^2/k^2 of the q integral. Making room for the next-to-leading order correction C, the result can be written:

$$\kappa = \frac{C_H g^4 T^3}{18\pi}\left(\left[N_{\rm c}+\frac{N_{\rm f}}{2}\right]\left[\ln\frac{2T}{m_D}+\xi\right]+\frac{N_{\rm f}\ln 2}{2}+\frac{N_{\rm c} m_D}{T}C+\mathcal{O}\left(g^2\right)\right). \tag{2.5}$$

Here $\xi = \frac{1}{2}-\gamma_E+\frac{\zeta'(2)}{\zeta(2)} \simeq -0.64718$. The leading order part of eq. (2.5) was given explicitly in [19] (it could also have been extracted from the nonrelativistic limit of earlier results [14, 20].) The dependence of the next-to-leading order correction on physical parameters is contained in the coefficient multiplying C, which itself is a pure number: all of the above-mentioned next-to-leading order corrections depend on physical parameters in the same way as an $\mathcal{O}(m_D/T)$ fraction of the gluon contribution to κ^{LO}.

Expression eq. (2.4) itself contains $\mathcal{O}(g)$ corrections, giving rise to a rather trivial contribution[2] to C, $C_{2\to 2} = \frac{21}{8\pi} \simeq 0.8356$. It arises wholly from the $k \sim gT$ region of the gluon contribution to eq. (2.4), where the result of the q integration is poorly described by the leading term of its m_D^2/k^2 expansion, which was used to obtain the leading order behavior eq. (2.5). Although slightly tedious, the evaluation of $C_{2\to 2}$ is entirely straightforward and we do not present it here. In section 4 we compute the difference between the full next-to-leading order momentum diffusion coefficient, and what is already incorporated in κ^{LO}, and obtain $\tilde{C} \simeq 1.4946$. Thus $C \equiv C_{2\to 2} + \tilde{C} \simeq 2.3302$.

Our result eq. (2.5) is plotted in figure 3. A simple-minded estimate of the regime of validity of perturbation theory can be given by equating the size of the correction to the size of the leading-order result. What is usually referred to in the literature as being the leading order result is eq. (2.4), numerically integrated at a given value of the coupling (this is the curve called "leading order" in figure 3): the correction becomes as large as this leading order result when $\alpha_{\rm s} \gtrsim 0.04$. This suggests that at that point perturbation theory starts to get into trouble. For this reason, and as should be clearly suggested by the plot, we do not believe that our calculation can be directly used as an "improvement" to the determination of κ in the context of heavy ion collisions, where phenomenologically realistic values of the coupling are in the range $\alpha_{\rm s} \sim 0.3 - 0.5$. Rather our results signal difficulties with the approach.

Nevertheless we would not like to sound overly pessimistic and conclude that our results signal that no prediction beyond $\alpha_{\rm s} = 0.05$ is possible. Rather, the real question now is

[2] In [15] this contribution was named $C_{\text{eq. (4)}}$.

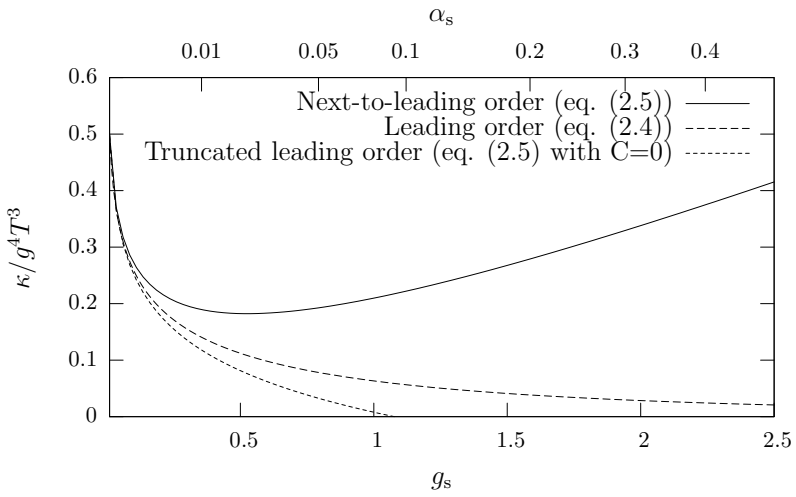

Figure 3: Comparison of leading and NLO results for $N_f = 3$ QCD as a function of coupling.

how large the higher order corrections are, and more pertinently, which parts of C may duplicate themselves in higher-order terms, in some more or less predictable (and therefore resummable) fashion.

Consider for instance the difference between the two lowest curves of figure 3, which is attributable to $C_{2\to2}$, up to terms which are of yet higher order in the m_D/T expansion of eq. (2.4). This contribution, which can be evaluated knowing only the tree-level matrix elements with massless external states (and HTL corrections resummed on the exchanged gluon), is better described as an "ambiguity" in the leading-order result rather than as a correction to it. This ambiguity is large because the Coulomb scattering processes against soft gluons (which give the small k contribution to eq. (2.4)) are poorly described by the leading term of an m_D/T expansion. This is unrelated to the question of whether these processes are correctly described by the right-hand side of κ^{LO}, which is the most pertinent question to ask if we are concerned with higher order terms. Actually, our calculation tells us that the effect of the HTL changes in the dispersion relation and interaction strength of the soft gluons is relatively modest, essentially given by the pole-pole contribution of section 4.3.4, of order $C_{(A),\mathrm{pole-pole}} \sim -0.20$. Thus it appears that this region of phase space is not so poorly described by eq. (2.4), and that simply defining this full expression to be the leading order result should provide a reasonable resummation of the contribution $C_{2\to2}$.

Along the same lines, there is another contribution to C which has a simple physical interpretation and which would be easy to include into the leading order calculation. As we will discuss in subsection 4.2, just over half of the remaining correction arises from a shift in the (real) Debye screened propagator $1/(q^2 + m_D^2)$ appearing in eq. (2.4). This can be understood as an NLO momentum dependence in the Debye screening mass m_D^2. This momentum dependence can be resummed in a few ways. One way would be to solve for it in the 3D Euclidean effective theory nonperturbatively or via a gap equation (though this approach appears to be special to heavy quark diffusion, where the exchange momentum

JHEP02(2008)081

is strictly spatial). Another method would be to replace m_D^2 in eq. (2.4) with the full momentum-dependent leading-order self-energy at general q (though this procedure does not appear to be gauge invariant).

For these reasons we think with some optimism that two thirds of the difference between the lowest and highest curves in figure 3 can be absorbed in a relatively simple systematic resummation scheme, and at most only one third represents complicated physics that will be really difficult to resum. Such a resummation scheme might then extend the reach of perturbation theory to $\alpha_{\rm s} \sim 0.15$ or so-high enough for almost all cosmological applications, though still not enough to be much use for heavy ion physics. Clearly such issues of resummation are an interesting problem for future work.

2.4 $\mathcal{N}$=4 super Yang-Mills

Results for heavy quark diffusion in the *strong* coupling regime of $\mathcal{N}$=4 super Yang-Mills (SYM) have been obtained in the literature, exploiting the AdS/CFT correspondence [21, 22]. It seems interesting to study the heavy quark momentum diffusion coefficient also at weak coupling in this theory, for the purpose of comparison between the two regimes and for comparison between this theory and ordinary QCD. The leading order result at weak coupling has previously been given [23], and here we present the next-to-leading order correction it receives.[3]

We begin with a brief description of $\mathcal{N}$=4 SYM and of heavy quarks in this theory. In addition to the gauge field A_μ, $\mathcal{N}$=4 SYM contains four Weyl fermions and six real scalars, all transforming under the adjoint representation of the gauge group. The theory contains a single dimensionless coupling constant g, which sets the strength of the gauge, Yukawa and scalar interactions; the Lagrangian is completely determined by the supersymmetry [24]. The strong coupling results are obtained in the large $N_{\rm c}$ limit of the theory with gauge group SU($N_{\rm c}$), and for this reason we will express our results in terms of the t'Hooft coupling $\lambda \equiv g^2 N_{\rm c}$. What is meant by a "heavy quark" in this theory is an $\mathcal{N}$=2 massive hypermultiplet added to it, transforming under the fundamental representation of the gauge group. In terms of the $\mathcal{N} = 2$ field content of $\mathcal{N}$=4 SYM, this heavy hypermultiplet is minimally coupled to the $\mathcal{N} = 2$ gauge multiplet of the theory, but is not directly coupled to the massless matter hypermultiplet. This is the conventional setup employed in AdS/CFT studies [21].

In the large mass $M \gg T$ limit, processes which would change the identity of the heavy particles, from heavy quarks to heavy scalars and vice-versa, are suppressed [23]. Thus the heavy fermion carries an approximately conserved U(1) charge and it makes sense to speak about its momentum diffusion coefficient, with no reference to its scalar superpartners. In addition to the scattering processes depicted in figure 1, in this theory at leading order there are scattering processes involving light scalars, depicted in figure 4. Including these

[3] We present our results at leading order in the large $N_{\rm c}$ expansion. Strictly speaking, the theory at finite $g^2 = \lambda/N_{\rm c}$ and with added fundamental matter has a Landau pole; however it is valid perturbatively. To generalize eq. (2.6) and eq. (2.7) to finite $N_{\rm c}$, multiply the righthand sides by $2C_H/N_{\rm c}$.

JHEP02(2008)081

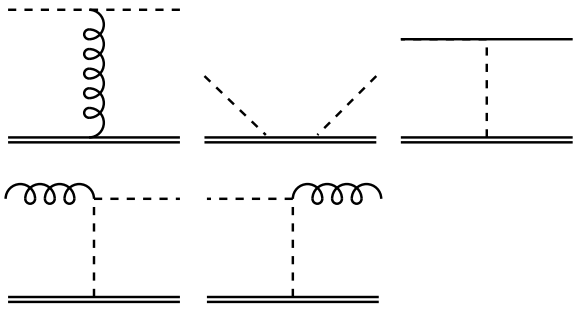

Figure 4: Leading order diagrams involving scalars, which are present in $\mathcal{N}$=4 SYM but not in QCD.

processes, the leading order momentum diffusion coefficient κ can be written [23]:

$$\kappa^{\rm LO}_{(SYM)} = \frac{\lambda^2}{24\pi^3}\int_0^\infty k^2 dk \int_0^{2k} q^3 dq \times \left\{ \begin{array}{l} n_B(k)(1+n_B(k))\left(2-\frac{q^2}{k^2}+\frac{q^4}{4k^4}\right)/\left(q^2+m_D^2\right)^2 \\ +n_B(k)(1+n_B(k))\left[\frac{5}{(q^2+m_D^2)^2}+\left(\frac{1}{q^2+m_D^2}-\frac{1}{2k^2}\right)^2\right] \\ +4n_F(k)(1-n_F(k))\left(2-\frac{q^2}{2k^2}\right)/\left(q^2+m_D^2\right)^2 \\ +2n_B(k)(1+n_B(k))\left(\frac{q^2}{k^2}-\frac{q^4}{4k^4}\right)/\left(q^2+m_S^2\right)^2 \\ +2n_F(k)(1-n_F(k))\frac{q^2}{k^2}/\left(q^2+m_S^2\right)^2 \,, \end{array} \right. \tag{2.6}$$

where $m_D^2 = 2\lambda T$ and $m_S^2 = \lambda T$. The first line describes Coulomb scattering against gluons, the second line describes Coulomb scattering against five real scalars and Coulomb plus Yukawa-Compton scatterings against one real scalar.[4] The third line is Coulomb scattering of fermions, the fourth line is the scalar-mediated conversion of light gluons to light scalars and vice-versa, and the last line contains the scalar-mediated scatterings against light fermions. The integrals of eq. (2.6) were evaluated to leading order in $m_D/T \sim \sqrt{\lambda}$ in [23]; making room for the next-to-leading order contribution the result can be written:

$$\kappa^{(SYM)} = \frac{\lambda^2 T^3}{6\pi}\left(\ln\frac{2T}{m_D} + \xi + \frac{1}{2} + \frac{1}{3}\ln 2 + \frac{\sqrt{2\lambda}}{6}C^{(SYM)} + \mathcal{O}\left(g^2\right)\right), \tag{2.7}$$

with ξ as defined below eq. (2.5). As for QCD, a rather trivial contribution $C_{2\to 2}^{(SYM)} = \frac{15}{2\pi} - \frac{3}{\pi\sqrt{2}} \simeq 1.7121$ to $C^{(SYM)}$ arises from the expansion of eq. (2.6) to next-to-leading order in $\sqrt{\lambda}$, coming from the $k \sim \sqrt{\lambda}T$ region of processes involving external bosons.

[4] Apparently the Yukawa-Compton scattering processes against scalars (the second diagram in figure 4) were not included in the calculation of Vuorinen and Chesler [23]. This caused an error in their determination of the constant term in eq. (2.7); they found $\frac{7}{12}$ rather than $\frac{1}{2}$.

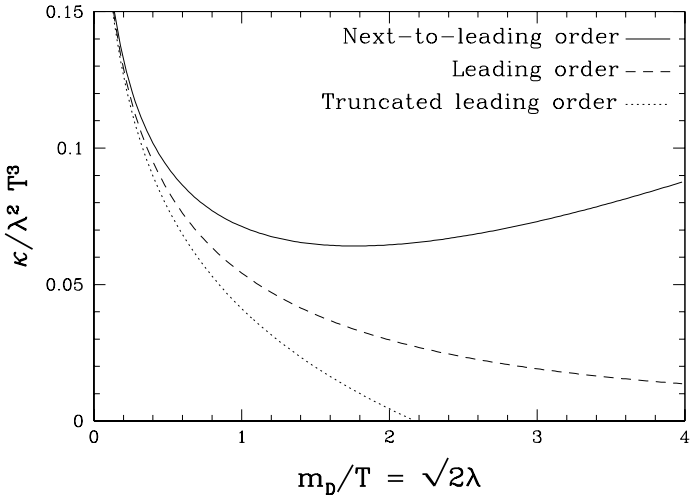

Figure 5: Comparison of next-to-leading and leading order results for heavy quark diffusion in $\mathcal{N}$=4 SYM theory.

Another part of C is precisely the same as the "difficult" part of the QCD calculation, $\tilde{C}^{(QCD)} \simeq 1.4946$. The remainder $\tilde{C}^{(SYM)} \simeq 0.19172$ is calculated in section 5. Thus $C^{(SYM)} = C_{2\to 2}^{(SYM)} + \tilde{C}^{(QCD)} + \tilde{C}^{(SYM)} \simeq 3.3984$.

This result is plotted in figure 5. As the figure shows, the convergence of the series is somewhat better than in QCD. Viewed as a function of the t'Hooft coupling λ the correction is 100% of the leading value for $\lambda \simeq 1.71$, to be compared with the QCD value of $\alpha_{\rm s} = 0.033$, which is $\lambda = 1.26$. Viewed as a function of the Debye screening scale, the comparative convergence in SYM would seem even better; the 100% correction point occurs for $m_D = 1.85T$, whereas it is $m_D = \sqrt{\frac{3}{2}}gT = 0.79T$. However, estimates of this kind can sometimes be deceptive: the fact that at fixed m_D/T the NLO correction in SYM is comparatively smaller than in QCD can be mostly attributed to the leading order result being stronger in SYM, due to its larger number of matter fields (which also scatter with a larger group theory factor, being in the adjoint representation.) However, this additional physics that is present in SYM suffers from relatively modest NLO corrections, the most severe corrections still being associated with soft gluons. Thus, although the leading order result has a wider range of validity in SYM than in QCD, it seems reasonable to expect the range of validity of the NLO correction itself to be roughly similar in SYM and QCD, in terms of m_D/T.

3. Effective theory and leading-order analysis

Our first step towards a rigorous analysis of the momentum diffusion coefficient κ is a non-perturbative definition [22] in terms of a force-force (electric field-electric field) correlator with Wilson lines connecting the electric fields:

$$\kappa \equiv \frac{g^2}{3d_H}\int_{-\infty}^{\infty} dt\, \mathrm{Tr}_H \langle W(t;-\infty)^\dagger\, E_i^a(t) t_H^a\, W(t;0)\, E_i^b(0) t_H^b\, W(0;-\infty)\rangle\,. \tag{3.1}$$

The trace runs over the representation of the gauge group of the heavy quark, and the Wilson lines W act on this representation. Intuitively, eq. (3.1) is exactly the force-force correlator of eq. (2.1), with the forces given by electric fields and the Wilson line representing the gauge rotation of the heavy quark due to propagation, which ensures gauge invariance. Because of operator ordering issues, the Wilson lines shown are not equivalent to connecting the E fields with an adjoint Wilson line. The Wilson lines also incorporate the effect of the heavy charge on the plasma (which is why they must go back to time $-\infty$). In general they introduce nontrivial representation dependence into the heavy quark diffusion constant, and in fact such Wilson lines are even required in QED (diffusion of ions in a QED plasma depends on the ionic charge Z in a more complicated way than Z^2 only because of these Wilson lines, which account for the reaction of the plasma to the presence of the charge). However we will see that to the order we work here, they can be replaced by an adjoint Wilson line.

Our approach is to calculate this correlation function within HTL effective field theory. This is an infrared effective description valid below a cutoff scale $\sim T$ which describes gauge fields and fermion fields, resumming into the Lagrangian certain $O(T^2)$ plasma effects. Perturbatively this introduces corrections to the propagators and vertices which become $O(1)$ at the scale $\sim gT$, which is a natural scale in HTL effective theory. The effective theory requires matching to the full thermal theory in the UV, requiring counterterms both in the Lagrangian parameters and in correlation functions such as eq. (3.1). Perturbation theory within the HTL effective theory is expected to converge in powers of g, which intuitively can be though of as the usual factor g^2 times a Bose statistical factor evaluated at the scale gT, $n_B(gT) \sim 1/g$. The HTL calculation can also encounter infrared divergences, arising from the unscreened low-frequency magnetic gluons. The appearance of such an IR divergence signals the breakdown of perturbation theory and the need for nonperturbative information about the ultrasoft magnetic sector. We expect such IR divergences at some finite order in perturbation theory, but this proves to be beyond the NLO level we consider here.[5]

Let us proceed with the leading order calculation of the correlator in eq. (3.1). At leading order one may replace the Wilson lines with identity operators and use the noninteracting form of the electric field correlator,[6] $E_i = \partial_i A_0 - \partial_0 A_i$. The time integral means we need the result at zero frequency and so the $\partial_0 A_i$ piece does not contribute.[7] Fourier transforming to the momentum basis, we rather immediately obtain

$$\kappa_{LO} = \frac{g^2 C_H}{3 d_A} \int \frac{d^3q}{(2\pi)^3} q^2 \langle A_{0a}(\omega = 0, q) A_{0a}(0) \rangle = \frac{g^2 C_H}{3} \int \frac{d^3q}{(2\pi)^3} q^2 G^{>}_{00}(0, q) \,. \tag{3.2}$$

The Wightman propagator is to be evaluated within the HTL effective theory. Using

[5] We believe that most transport coefficients are sensitive to nonperturbative magnetic physics at $\mathcal{O}(g^2)$, which is the relative contribution of these magnetic fields to transverse momentum diffusion for a moving particle ($v \sim 1$) in the soft electromagnetic fields of the HTL effective theory. Because the heavy quark considered here has $v \ll 1$, we believe magnetic physics arises at a higher order than $\mathcal{O}(g^2)$.

[6] We work in $[-+++]$ metric contentions and 4-vector potential $A^\mu = (A^0, A^i)$ with A^0 the usual scalar and A^i the usual vector potentials.

[7] This does not apply in gauges such as temporal gauge where the zero frequency gauge boson propagator can display singularities.

the KMS condition we can express the Wightman propagator in terms of the retarded propagator,

$$G^{>}(\omega,q) = 2(n_B(\omega)+1)\,\mathrm{Re}\,G_R(\omega,q) \tag{3.3}$$

which is given in the HTL effective theory, in strict Coulomb gauge (which we use throughout), by

$$\begin{aligned} G_R^{00}(P) &= \frac{i}{p^2+\Pi_R^{00}(P)}, \\ G_R^{T}(P) &= \frac{-i}{P^2+\Pi_R^{T}(P)}. \end{aligned} \tag{3.4}$$

with

$$\begin{aligned} \Pi_R^{00}(P) &= m_D^2\left[1-\frac{\eta}{2}\ln\left(\frac{|1+\eta|}{|1-\eta|}\right)+\frac{i\pi\eta}{2}\theta\left(1-\eta^2\right)\right] \\ \Pi_R^{T}(P) &= m_D^2\left[\frac{\eta^2}{2}+\frac{\eta(1-\eta^2)}{4}\ln\left(\frac{|1+\eta|}{|1-\eta|}\right)-\frac{i\pi\eta(1-\eta^2)}{4}\theta\left(1-\eta^2\right)\right], \end{aligned} \tag{3.5}$$

where $\eta \equiv p^0/p$. Therefore the leading order momentum diffusion coefficient is

$$\kappa^{LO} = \lim_{\omega\to 0}\frac{g^2C_H}{3}\int\frac{d^3q}{(2\pi)^3}q^2\frac{2T}{\omega}\frac{\pi\omega m_D^2}{2q(q^2+m_D^2)^2} = \frac{g^2C_Hm_D^2}{6\pi}\int\frac{q^3dq}{(q^2+m_D^2)^2}\,. \tag{3.6}$$

This integral is UV log divergent, indicating the need to perform a matching calculation. This is done by finding the result in the full theory, which gives eq. (2.4) (without the m_D^2 terms in the denominator). In the range $gT \ll q \ll T$ the two calculations agree; performing the k integration in eq. (2.4) treating $q \ll k$ reproduces eq. (3.6). The matching should be performed in some way so that the UV region is equivalent to eq. (2.4) and the IR region is equivalent to eq. (3.6). One way of doing this would be to compute both eq. (2.4) (without m_D^2 factors in denominators) and eq. (3.6) each in dimensional regularization and add them; the $1/\epsilon$ factors will cancel and the finite parts will give a consistent leading order result [25]. Alternately one can simply insert m_D^2 factors in the denominators in eq. (2.4) (as has already been done) so that one expression is appropriate in the IR and UV. The error thus introduced at large q is only NNLO ($\mathcal{O}(g^2)$) and will not interfere with our NLO calculation.

4. Details of the calculation

We now proceed to push the leading order calculation of the last section to the next order in HTL perturbation theory.

4.1 Formalism and diagrams

The real-time correlator eq. (3.1) can be expressed in terms of correlators of fields ordered along the Schwinger-Keldysh contour [6, 26]. We find it convenient to use the Keldysh or ra basis (where one works in terms of the contour averaged or r and contour differenced or a fields rather than the fields on the upper 1 and lower 2 contours). Throughout we

Symbol	Notation	Expression for a free scalar field
r ← a	$G_{ra}(P) \equiv G_R(P)$	$\frac{-i}{P^2 - i\epsilon p^0}$
a → r	$G_{ar}(P) \equiv G_A(P)$	$\frac{-i}{P^2 + i\epsilon p^0}$
r ‖ r	$G_{rr}(P)$	$2\pi\delta(P^2)\left(\frac{1}{2} + n_B\left(\lvert p^0\rvert\right)\right)$

Table 1: Graphical notation for real-time propagators in the Keldysh basis, and their expression for a free scalar field. In all cases the momentum P flows from right to left.

will be using a graphical notation for the propagators of this formalism, summarized in table 1. We draw retarded (ra) and advanced (ar) propagators with an arrow on them, which points in the direction of the flow of time (thus towards the r index.) We draw the rr propagators with a double cut in the middle of it; there exists no aa propagator in this formalism. If one thinks of an rr propagator as carrying two outgoing arrows, leaving away from the cut, then an r field at a vertex will have an incoming arrow on it and an a field will have an outgoing arrow, leaving the vertex. Thus the ra assignments of the fields at the vertices can be readily recovered from our notation. The nonzero (tree-level) vertices in the Keldysh basis carry odd numbers of a indices, thus have an odd number of arrows leaving them (but arbitrarily many r indices, or incoming arrows.) Interaction vertices with one a index are precisely the same as the usual ones given in textbooks on quantum field theory at zero temperature, and those having three a indices are smaller by a factor $\frac{1}{4}$. This notation is the same as in [27].

Diagrammatic rules that generate the HTL effective vertices have recently been worked out for real time field theory in this basis [27]; we use the results and notation of that work, which are summarized in figure 6. In the HTL limit the hard degrees of freedom behave like classical point-like particles, which we draw as solid lines. The vertices (a) and (c) and the eikonal propagator (d) of the figure together describe the generation and propagation of disturbances of the hard particles' distribution functions in a background gauge field, and the two-point vertex (b) describes how these disturbances source gauge fields. These effects depend on the four-velocity $v^\mu = (1, \mathbf{v})$, $\mathbf{v}^2 = 1$, of the hard particle, which has to be averaged over for every connected solid line that appears in a diagram; a factor of m_D^2/T must also be included. The rr propagator (e) describes statistical fluctuations in the number density of the charges, and enters precisely once in the calculation of HTL amplitudes with two external a gluons. The only HTL three point vertex that exists has the ra assignment shown in (c); there exist no HTL amplitudes with more than two external a gluons. Diagrams containing self-energy insertions on gluon propagators must be discarded, since we are already using the HTL-resummed gluon propagators eq. (3.4). The application of these rules reproduces calculations in classical Yang-Mills plasmas with point-like (nonabelian) charges; more details can be found in [27].

In the Keldysh basis, correlators involving Keldysh a fields with soft momenta $p \sim gT$ are systematically down by powers of g, relative to similar correlators with Keldysh r fields (see e.g. [27]), implying that at NLO all fields entering eq. (3.1) can be taken to be Keldysh

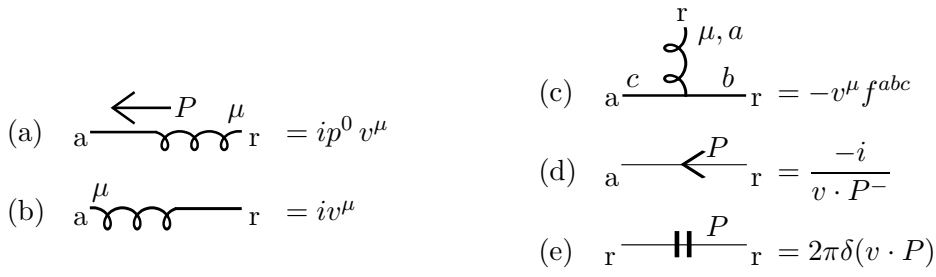

Figure 6: Feynman rules for the HTL theory, with ra indices explicitly shown: (a)-(c) give interaction vertices and (d)-(e) give effective propagators for classical particles. All two-point functions are proportional to the identity in color space, δ^{ab}, not explicitly shown. A factor (m_D^2/T) plus an integration $\int \frac{d\Omega_v}{4\pi}$ over the four-velocity v^μ must be assigned to every disjoint solid line appearing in a diagram.

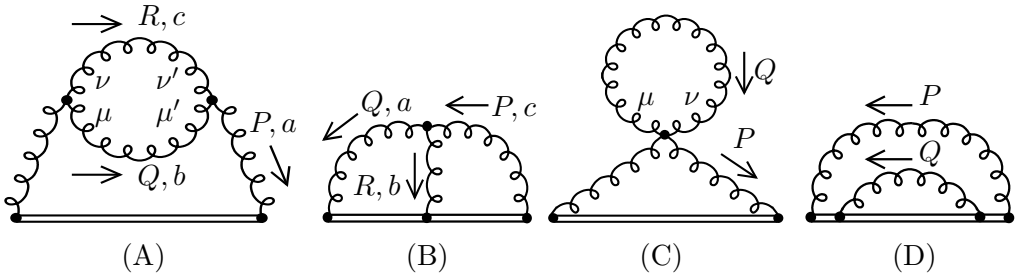

Figure 7: The Feynman diagrams that contribute to $\kappa^{\rm NLO}$, with assignments of momenta, Lorentz and color indices. All propagators are soft and HTL-resummed, and all interaction vertices include HTL corrections; the arrows denote only the momentum flow. The Lorentz indices of the gluons which connect to the heavy quark (shown as the double line) are all "0".

r fields. This means that operator ordering issues actually are subleading, and that at NLO the Wilson lines in eq. (3.1) can be traded for a single adjoint Wilson line.

It is convenient to write the electric field operators as $E^i = -\partial^i A^0 - D_t A^i$. Using the equation of motion for a Wilson line, $D_t W(t;0) = 0$, we can then express

$$W(t;0)^\dagger \left(D_t A^{ia}(t)\, t_h^a\right) W(t;0) = \frac{d}{dt}\left(W(t;0)^\dagger\, A^{ia}(t)\, t_h^a\, W(t;0)\right) , \tag{4.1}$$

which contributes a total derivative to eq. (3.1) and can be dropped.[8] Therefore the E^i can be replaced with $-\partial^i A^0$, and the desired correlation function becomes

$$\kappa = \frac{C_H g^4}{3 d_A} \int_{-\infty}^{\infty} dt\, \langle \partial^i A^{0\,a}(t) \left[\mathcal{P} e^{[\int_0^t dt' A^0(t'),\cdot]}\right]_{ab} \partial^i A^{0\,b}(0)\rangle \, . \tag{4.2}$$

Expanding the Wilson line gives a series of correlators of A^0 fields. The diagrams we need at NLO are shown in figure 7.[9] These diagrams are to be evaluated within the HTL

[8] This is true in any gauge in which the propagators show no divergent or pathological behavior in the zero-frequency limit. These includes the covariant or Coulomb gauges, but not the temporal axial gauge.

[9] There is also a diagram which looks like (D) but with crossed gluon lines. It vanishes by rotational invariance.

JHEP02(2008)081

effective theory, meaning that all propagators are HTL resummed and all vertices include HTL vertices — except for the vertices on the Wilson line, shown as the double line in the diagram. Naively there could be two more diagrams, corresponding to (A) and (C) but with fermions rather than gauge bosons in the loops; but these are suppressed by at least one factor of $n_f/n_b \sim g$ relative to the indicated diagrams and can be neglected at NLO.

4.2 Real part of self-energy diagrams (A) and (C)

Diagrams (A) and (C) of figure 7 correspond to NLO self-energy corrections to the soft zero-frequency longitudinal gluon propagator, and can be decomposed into real and imaginary parts. We begin with the real part of the self-energy. Since it is needed only at zero frequency, it can be most convenient evaluated within the imaginary time formalism, in which the frequency integrals are replaced by discrete sums over the (imaginary) Matsubara frequencies $\omega_n = 2\pi nT$, n integer [28]. In this formalism, no analytic continuation of any kind is required at *zero* external frequency, and we can directly analyze the discrete sum over the Matsubara frequencies.

Because the HTL effective vertices vanish when all of their external frequencies are zero, and are subleading by g^2 (and at any rate, inappropriate) when one of their external momenta carries a nonzero Matsubara frequency $|\omega_n| \gtrsim T$, the diagrams involving HTL vertices do not contribute at NLO. Similar cancellations occur for the transverse-transverse contribution with tree interaction vertices, because the relevant interaction vertex vanishes when all frequencies are zero, and the contribution of nonzero Matsubara frequencies only receives $\mathcal{O}(g^2)$ corrections (the presence of the hard frequency scale ω_n in the loop propagators ensures that the self-energy corrections on the loop propagators are down by $\mathcal{O}(g^2)$, and that the p dependence of the integral over spatial momenta can be expanded into integer powers of p^2/T^2 when $p \ll T \lesssim \omega_n$.) The diagrams with topology (C), involving four-point vertices, similarly do not contribute: the one with an HTL vertex is irrelevant at zero external frequency, and when the vertex is a tree vertex the propagator in the loop must be purely transverse (in the strict Coulomb gauge) since there is no interaction vertex involving only A^0 fields; but the HTL correction to this propagator at zero frequency vanishes. These simplifications, which are specific to the zero-frequency retarded self-energy (and to a lesser extent, to our use of strict Coulomb gauge), are perhaps best understood in terms of the dimensionally reduced effective theory [29].

We are thus left to evaluate the transverse-longitudinal loop with tree-level interaction vertices and HTL-resummed propagators. Only the contribution from the zero Matsubara frequency is needed,

$$\begin{aligned}\delta\Pi_R^L(p) &= -g^2 N_c T \int_q 4p^2 \left(1 - \frac{(p\cdot q)^2}{p^2 q^2}\right) \frac{1}{q^2}\frac{1}{r^2 + m_D^2} \\ &= -\frac{g^2 N_c T}{2\pi}\left[m_D + \frac{p^2 - m_D^2}{p}\tan^{-1}\left(\frac{p}{m_D}\right)\right], \end{aligned} \tag{4.3}$$

where $\int_q$ is shorthand for $\int \frac{d^3q}{(2\pi)^3}$ and where the arctangent takes values in $[0, \frac{\pi}{2}]$. The same result could also have been obtained within the real-time formalism, albeit with somewhat

more work. This $\mathcal{O}(g)$ correction to the real part of the longitudinal gluon self-energy induces an $\mathcal{O}(g)$ correction to κ,

$$\delta\kappa_{\rm Re} = \frac{C_H g^2}{3}\int_p p^2 \Pi^{>\,00}(p)\left[\frac{1}{(p^2+m_D^2+\delta\Pi_R^L(p))^2}-\frac{1}{(p^2+m_D^2)^2}\right] \tag{4.4}$$

which, using the HTL approximation $\Pi^{>\,00}(p) = m_D^2\pi T/p$, yields a contribution to the dimensionless coefficient C from eq. (2.5):

$$\begin{aligned} C_{(A),{\rm Re}} &= 6\pi\int_p \frac{p}{(1+p^2)^3}\left[1+\frac{p^2-1}{p}\sin^{-1}\left(\frac{p}{\sqrt{1+p^2}}\right)\right] \\ &= \frac{3}{2\pi}\left(1+\frac{\pi^2}{16}\right) \simeq 0.77198914\ldots \end{aligned} \tag{4.5}$$

where we have rescaled p to p/m_D. Note that the integral is both IR and UV safe.

4.3 Self-energy (A): imaginary part

4.3.1 Overview of the calculation

The imaginary part of the gluon self-energy diagram (A) is probably the most technically challenging part of this calculation. Instead of calculating the ($\mathcal{O}(p^0)$ term of the) imaginary part of the retarded self-energy, we find it more convenient to calculate directly the Wightman self-energy $\Pi^{>\,00}(P) = 2(1+n_B(p^0))\,{\rm Im}\,\Pi_R^{00}$, which can be evaluated directly at zero frequency. There exists a finite temperature cutting rule, analogous to the familiar zero-temperature Cutkowski rule, which expresses this function in terms of a sum over diagrams that are divided into two parts by one cut [30, 31].[10] The propagators traversed by the cut are to be evaluated as Wightman propagators, $G^>(P) \equiv (G_R(P)-G_A(P))(1\pm n(p^0))$, for bosons and fermions respectively, and the "amplitudes" on each side of the cut are to be evaluated as the fully-retarded amplitudes of the real-time formalism, the retardation (e.g. time flow) being taken to be away from the cut, toward the external legs. In terms of the Keldysh ra basis, this means that all cut propagators attach to the neighboring vertices like Keldysh r fields, and external legs of the self-energy diagram should be considered as carrying Keldysh a indices. These fully-retarded amplitudes are the simplest analytic continuation of the imaginary-time amplitudes [32] (they are obtained by continuing all but one of the external momenta from the upper-half complex frequency plane.) A direct proof of the rule we use, within the real-time formalism, has also been given using the R/A formalism [33] (see also [34], section 3.6.); the cutting rule presented there is the same as the one we use, since the fully retarded amplitudes of the ra and R/A formalisms are the same.[11]

[10] Although the rules given by these authors deal with the imaginary part of the retarded self-energy, rather than the Wightman self-energy, the rule we use follows from the latter by a straightforward application of fluctuation-dissipation relations (KMS conditions).

[11] Since the most complicated self-energy diagram we need to evaluate contains "only" three loops, it is also possible to give a direct proof of the cutting rule in our case, starting from the standard rules of the Schwinger-Keldysh ra formalism applied to the calculation of the aa self-energy (which is the average of the two Wightman self-energies.) We have checked this; although somewhat long the proof is a succession of simple manipulations, which only involve the addition or subtraction of suitable closed loops of retarded propagators to the diagrams (such closed loops in a diagram evaluate to zero.)

JHEP02(2008)081

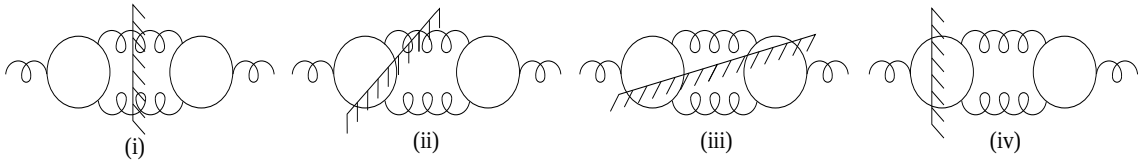

Figure 8: The distinct cuts which can go through the self-energy diagram (A) of figure 7 with two HTL effective vertices (drawn as loops), as explained in the text. Solid lines denote hard propagators and the two gluon propagators carry soft momenta.

The four distinct types of cuts which contribute to the self-energy diagrams with two HTL effective vertices are depicted in figure 8. As just mentioned, all cut propagators are Wightman propagators, and they attach to the neighboring vertices like Keldysh r fields. When soft gluon propagators are traversed by the cut, the small P approximation $G^{>}(P) \approx G_{rr}(P)$ can be used. When HTL vertices are traversed by the cut, two hard propagators are put on-shell; as discussed in more detail in [27], the corresponding amplitudes are precisely given by the real-time HTL amplitudes having two external Keldysh a indices. Physically, these amplitudes are obtained by making the eikonal approximation in all propagators and vertices entering in the hard loop; the interested reader may readily verify that this reproduces the HTL amplitudes with two Keldysh a indices as given by the rules of section 4.1.

The cuts of type (i)-(iii) share a feature which is very pleasing from the viewpoint of their numerical evaluation: they are given by expressions supported on the spectral weights of the soft gluon propagators. In other words they split into pole-pole, pole-cut and cut-cut parts, according to whether the momenta Q and R are restricted to lie on the position of a plasmon pole, or to lie within the space-like region ("Landau cut"). This should be obvious from figure 8. In contrast, cut (iv), which represents a (two-loop!) virtual correction to the tree processes considered in section 2.2, might be expected to induce additional complications since it leaves essentially unconstrained the gluon momenta that appear in it. However, somewhat to our surprise, under the special circumstance $p^0 = 0$ we were able to bring this contribution into a form manifestly supported within the cut-cut region. The relevant manipulations are described below in greater detail. As far as we know, this additional difficulty did not show up in previous HTL calculations, such as Braaten and Pisarski's pioneering evaluation of the gluon damping rate [35], or Braaten, Pisarski and Yuan's calculation of soft dilepton production [36], cut (iv) being kinematically forbidden in these cases due to the the external momentum being time-like.

4.3.2 Evaluation of the cuts

In figure 9 we give explicit expressions for the HTL effective vertices entering figure 8 (i)-(iii), in terms of certain functions,

$$M^{\mu\nu}(Q,R) \equiv \int \frac{d\Omega_v}{4\pi} \frac{v^\mu v^\nu}{v\cdot Q^- v\cdot R^-}\,, \tag{4.6}$$

$$K^{\mu\nu}(Q,P) \equiv \int \frac{d\Omega_v}{4\pi} i\pi\delta(v\cdot Q)\frac{v^\mu v^\nu}{v\cdot P^-}\,, \tag{4.7}$$

(1) 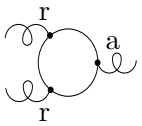

$$= m_D^2 g\, i^2(-i)^2 f^{a'bc} \int_v \frac{v^{\mu'} v^{\nu'}}{v\cdot P^-}\left[\frac{q^0}{v\cdot Q^-} - \frac{r^0}{v\cdot R^-}\right]$$
$$\equiv m_D^2 g f^{a'bc} \times q^0 M^{\mu'\nu'}(Q,R)$$

(2) 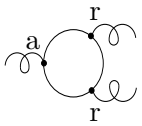

$$= m_D^2 g f^{abc} \times -q^0 M^{\mu\nu}(Q,R)^*$$

(3) 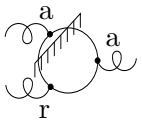

$$= m_D^2 g T\, i^3 f^{a'bc} \int_v \frac{v^{\mu'} v^{\nu'}}{v\cdot P^-} 2\pi\delta(v\cdot R)$$
$$\equiv m_D^2 g f^{a'bc} \times -2K^{\mu'\nu'}(R,P)$$

(4) 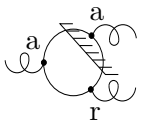

$$= m_D^2 g f^{abc} \times 2K^{\mu\nu}(Q,P)^*$$

Figure 9: The HTL effective vertices that appear in figure 8 (i)–(iii), with ra indices shown. The momenta, Lorentz and color indices are as suggested by the position of these objects in figures 7, 8.

$$V^{\mu\nu}(Q,R) = \frac{-1}{m_D^2}\left[2q^0\eta^{\mu\nu} + (R+P)^\mu \eta^{\nu 0} - (Q+P)^\nu \eta^{\mu 0}\right] . \tag{4.8}$$

which are related to the fully retarded HTL three-point vertex, its discontinuities, and to the tree vertex, respectively. The Keldysh indices that appear on these effective vertices, for the cuts (i)-(iii), are completely determined by the cutting rule we use.

With these basic building blocks in hands, the evaluation of the cuts of type (i)-(iii) is relatively straightforward (our normalization is $\Pi^{>\,00}(P) = 2\,\mathrm{Im}\,\Pi_R^{00}(P)(T/p^0)$ with Π_R^{00} as in eq. (3.4):

$$\begin{aligned}
\frac{\Pi^{>\,00}_{(A),(\mathrm{i})}(p)}{N_c m_D^4 g^2 T^2/2} &= \int_Q M_{\mu\nu}(Q,R) M_{\mu'\nu'}(Q,R)^*\, \rho^{\mu\mu'}(Q)\rho^{\nu\nu'}(-R)\,,\\
\frac{\Pi^{>\,00}_{(A),(\mathrm{ii})}(p)}{N_c m_D^4 g^2 T^2/2} &= \int_Q \Big[-2M_{\mu\nu}(Q,R) K_{\mu'\nu'}(Q,P)^*\, G_R^{\mu\mu'}(Q)\rho^{\nu\nu'}(-R)\\
&\qquad +2K_{\mu\nu}(Q,P) M_{\mu'\nu'}(Q,R)^*\, G_A^{\mu\mu'}(Q)\rho^{\nu\nu'}(-R)\Big]\\
&\qquad +(Q\leftrightarrow R)\,,\\
\frac{\Pi^{>\,00}_{(A),(\mathrm{iii})}(p)}{N_c m_D^4 g^2 T^2/2} &= \int_Q 4K_{\mu\nu}(R,P) K^*_{\mu\nu'}(Q,P)\, G_R^{\mu\mu'}(Q) G_A^{\nu\nu'}(R)\\
&\qquad +(Q\leftrightarrow R)\,,
\end{aligned} \tag{4.9}$$

all of which are manifestly real. We are using the approximation $G_{rr}(Q) \approx \rho(Q)/q^0$, with $\rho \equiv (G_R - G_A)$ being the spectral density. The contribution from cut (i) is also manifestly positive, as expected from its rather obvious interpretation as the square of a one-loop amplitude (although at this stage it might not be obvious that the sum over Lorentz indices yields a sum of positive terms; this is confirmed in section 4.3.3.) In eq. (4.9) the contribution from diagrams involving the tree interaction vertices is not shown explicitly; it can be recovered by the simple substitution, for each appearance of the fully retarded

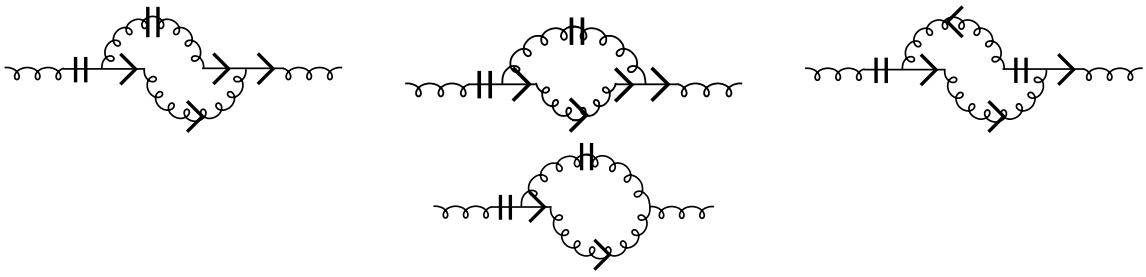

Figure 10: Zoom on the *ra* structure of the propagators appearing in the HTL diagrams contributing to cut (iv) of figure 8.

HTL vertex $M_{\mu\nu}(Q,R)$ or its complex conjugate,

$$q^0 M_{\mu\nu}(Q,R) \to q^0 M_{\mu\nu}(Q,R) + V_{\mu\nu}(Q,R)\,. \tag{4.10}$$

Evaluating the cuts of type (iv) poses some additional difficulty, as mentioned above. The HTL diagrams contributing to it are depicted in figure 8. The leftmost solid line in these diagrams can be identified with the cut hard loop on the left-hand side of diagram (iv) in figure 8, collapsed to a one-dimensional line [27]: the cut (rr) HTL propagator replaces the two cut hard propagators in figure 8 (iv), and the retarded HTL propagator on its right replaces the (eikonalized) third propagator of this hard loop. The reason why there appears exactly one cut gluon, or HTL propagator, in the rest of the diagram is because the object which stands on the right-hand side of the explicit cut in figure 8 (iv) is a one-loop retarded amplitude (in the HTL theory.) The direct evaluation of these HTL diagrams yields:

$$\begin{aligned}\Pi^{>\,00}_{(A),(\mathrm{iv})}(P) \,=\, +2\,\mathrm{Re}\,N_c m_D^4 g^2 T^2 \int_Q 2K_{\mu\nu}(P,Q) \\ \times \begin{cases} M_{\mu'\nu'}(Q,P) G_R^{\mu\mu'}(Q)\rho^{\nu\nu'}(R)\dfrac{q^0}{r^0} \\ -M_{\mu'\nu'}(R,P) G_R^{\mu\mu'}(Q)\rho^{\nu\nu'}(R)\dfrac{r^0}{r^0} \\ -2K_{\mu'\nu'}(R,P) G_R^{\mu\mu'}(Q) G_A^{\nu\nu'}(R) + V_{\mu'\nu'}(Q,P) G_R^{\mu\mu'}(Q)\rho^{\nu\nu'}(R)\frac{1}{r^0}\,. \end{cases}\end{aligned} \tag{4.11}$$

Using standard methods of contour integration that make use of the analyticity of the prefactor $K_{\mu\nu}(P,Q)$ in the upper half q^0 plane, this expression can be rewritten more compactly. Specifically, we introduce a small $i\epsilon$ prescription $1/r^0 \to 1/(r^0 - i\epsilon)$ in all places this appears. This is equivalent to displacing the contour of r^0 integration slightly below the real axis (or, equivalently, the contour of q^0 integration slightly above the real axis), and does not change the final answer since the numerator vanishes at $r^0 = 0$, $\rho(R)$ being an odd function of r^0. However, the introduction of this prescription makes it possible to decompose $\rho(R)$ into $(G_R(R) - G_A(R))$, the integral of each term remaining well-defined. Decomposing also $2K(R,P)$ into $(M(R,P) + M(-R,P))$, and dropping all terms which

are analytic in the upper-half q^0 plane, one obtains:

$$\Pi^{>00}_{(A),(\mathrm{iv})}(P) \,=\, +2\,\mathrm{Re}\, N_c m_D^4 g^2 T^2 \int_Q 2K_{\mu\nu}(P,Q) G_R^{\mu\mu'}(Q) G_R^{\nu\nu'}(R) \times \left\{ \frac{q^0 M_{\mu'\nu'}(Q,P) - r^0 M_{\mu'\nu'}(R,P)}{r^0 - i\epsilon} + \frac{V_{\mu'\nu'}(Q,P)}{r^0 - i\epsilon} \right\}. \quad (4.12)$$

Although eq. (4.12) is valid for arbitrary p^0, a great simplification occurs when $p^0 = 0$: the denominator $1/(r^0 - i\epsilon)$ is antisymmetric under $Q \leftrightarrow R$, modulo its $i\epsilon$ prescription. By enforcing symmetry of the integrand under $(Q \leftrightarrow R)$ we can thus trade the prefactor $2K(P,Q)$ (whose support extends to $q^0 \to \infty$, a nuisance for numerical work) into the better-behaved combination $K(P,Q)+K(P,R) = 2\,\mathrm{Re}\, K(Q,R)$, whose support lies entirely within the region of spacelike Q and R, $|q^0| < \min(q,r)$. Due to the explicit factor of q^0 present in the numerator, the $i\epsilon$ prescription in the denominator of the HTL terms (the one involving $M_{\mu'\nu'}$) actually is unimportant and can be discarded, allowing $(Q \leftrightarrow R)$ symmetry to be enforced at no cost. However, no such factor of q^0 multiplies the term involving the tree vertex $V_{\mu'\nu'}$, and enforcing the $(Q \leftrightarrow R)$ symmetry in it gives rise to an additional contribution proportional to $\delta(q^0)$, coming from the mismatch of $i\epsilon$ prescriptions. Thus at $p^0 = 0$ eq. (4.12) becomes:

$$\frac{\Pi^{>00}_{(A),(\mathrm{iv})}(p)}{N_c m_D^4 g^2 T^2/2} \,=\, -8\,\mathrm{Re} \int_Q \left[\mathrm{Re}\, K_{\mu\nu}(Q,R)\right] G_R^{\mu\mu'}(Q) G_R^{\nu\nu'}(R) \left[M_{\mu'\nu'}(Q,R) + \frac{V_{\mu\nu}(Q,R)}{q^0} \right] -4 \int_q V_{i0}(q,r) G_R^T(q) G_R^{00}(r) \left(\delta^{ij} - \frac{q^i q^j}{q^2} \right) \mathrm{Im}\left[K_{j0}(p,q) - K_{j0}(p,r) \right] . \quad (4.13)$$

We remark that the apparent singularity at q^0, in the term involving the tree vertex on the first line, is illusory (this is why we dropped the $i\epsilon$ prescription in it.) Indeed, since the tree vertex with three A^0 fields is identically zero, and the tree vertex between one A^0 and two transverse gauge fields is explicitly proportional to q^0, a singularity could only happen when one gluon is transverse and the other one is longitudinal. However, in that case the prefactor $\mathrm{Re}\, K_{i0}(Q,R)$ turns out to be explicitly proportional to q^0. In terms of the formulae for the Lorentz algebra given in the next section, the corresponding statement is that $X_{T-L} \propto q^0$. Thus the first line of eq. (4.13) is not sensitive to the $q^0 \to 0$ region. However, although the prefactor $\mathrm{Re}\, K_{i0}(Q,R) = \frac{1}{2}(K_{i0}(P,Q)+K_{i0}(P,R))$ vanishes at $q^0 = 0$, $K_{i0}(P,Q)$ itself does not. This is the reason why one gets a nonzero residue at $q^0 = 0$ in the transverse-longitudinal case (and only in that case), as given on the second line of eq. (4.13).

To bring these expressions into a form suitable for numerical evaluation, we find it convenient to decompose all individual factors into their real and imaginary parts. Doing

so, the contributions eq. (4.9) and the first line of eq. (4.13) add up to ($\rho = 2\,\mathrm{Re}\,G_R$):

$$\frac{\Pi^{>\,00}_{(A)}(P)}{N_c m_D^4 g^2 T^2/2} = \int_Q \left\{ \begin{array}{l} \rho(Q)\rho(-R)\,\left[(\mathrm{Re}\,M - \mathrm{Re}\,K)^2 - (\mathrm{Im}\,K_Q)^2 \right. \\ \qquad\qquad \left. -(\mathrm{Im}\,K_R)^2 + (\mathrm{Re}\,K)^2\right] \\ +4\,\mathrm{Im}\,G(Q)\rho(R)\,[(\mathrm{Re}\,M - \mathrm{Re}\,K)\,\mathrm{Im}\,K_Q + \mathrm{Re}\,K\,\mathrm{Im}\,K_R] \\ +4\rho(Q)\,\mathrm{Im}\,G(R)\,[(\mathrm{Re}\,M - \mathrm{Re}\,K)\,\mathrm{Im}\,K_R + \mathrm{Re}\,K\,\mathrm{Im}\,K_Q] \\ +8\,\mathrm{Im}\,G(Q)\,\mathrm{Im}\,G(R)\,[(\mathrm{Re}\,M - \mathrm{Re}\,K)\,\mathrm{Re}\,K \\ \qquad\qquad - \mathrm{Im}\,K_Q\,\mathrm{Im}\,K_R]\,. \end{array} \right. \tag{4.14}$$

Here we have not explicitly written the contributions involving tree vertices, which are recovered by the simple substitution eq. (4.10), and we have dropped all Lorentz indices, which play no crucial role here. We are using the abbreviations $M \equiv M(Q,R)$, $K_Q \equiv K(Q,P)$ and $K_R \equiv K(R,P)$. This expression incorporates a wealth of real and virtual physical processes, as discussed in subsection 2.2.

In addition to eq. (4.14) we have the contribution from the $q^0 = 0$ residue, given by the second line of eq. (4.13). Using eq. (4.8) for V_{i0} and performing the v integration we can make the latter more explicit:

$$\frac{\Pi^{>\,00}_{(A),q^0=0}(P)}{N_c m_D^4 g^2 T^2/2} = \frac{8\pi}{m_D^2 p}\int_q \frac{1}{q^2(r^2+m_D^2)}\frac{p\cdot q}{q^2} = \frac{1}{m_D p}\left[\frac{\tan^{-1}\left(\frac{p}{m_D}\right)}{m_D p} - \frac{1}{p^2+m_D^2}\right]. \tag{4.15}$$

Here we performed the $\mathbf{q}$ integration by first doing the integration over the angle between $\mathbf{q}$ and $\mathbf{p}$, and then evaluating the integration over the magnitude q from its discontinuities at its branch cuts at $q = \pm p + i[m_D, \infty)$. This zero-frequency contribution to eq. (4.13) may appear odd-looking, compared to eq. (4.25). However, what we regard as truly remarkable, is the fact that the contribution from cut (iv) (a two-loop virtual correction!), *could*, when $p^0 = 0$, be cast into a computer-friendly form supported on the spectral weights of the gluon propagators. The leftover piece eq. (4.15) seems to be the price to pay for this welcomed simplification. It is not clear to the authors whether such a structure persists for general spacelike P with $p^0 \neq 0$.

4.3.3 The Lorentz structure

We have to sum over the Lorentz indices in expressions of the form

$$M_{\mu\nu}(Q,R)G^{\mu\mu'}(Q)G^{\nu\nu'}(R)M^*_{\mu'\nu'}(Q,R)\,. \tag{4.16}$$

This is where our choice of strict Coulomb gauge becomes particularly convenient. First, in this gauge the retarded and cut propagators have the same Lorentz structure, see eq. (3.4). Second, in this gauge the propagator decomposes into a longitudinal part G^{00} and two spatial, strictly transverse components, $G_{ij} = G^T(\epsilon_i\epsilon_j + \epsilon'_i\epsilon'_j)$. We can choose one of these components, say, ϵ, to lie in the plane defined by $\mathbf{q}$ and $\mathbf{r}$ and the other, ϵ', to be orthogonal to this plane.

These three components of the gauge propagator will give rise to four structures in evaluating eq. (4.16); one contribution proportional to $(G^{00})^2$, one contribution proportional to $G^{00}G^T$, and two contributions proportional to $(G^T)^2$, one of which arises from the out of plane and one from the in-plane polarization states.

The doubly longitudinal contribution to eq. (4.16) is trivial; it is $|M^{00}|^2 G^{00}(Q)G^{00}(R)$. Consider next the $G^{00}(R)G^T(Q)$ contribution. To evaluate the contribution we need to study $M_{i0}(Q,R)$, which, viewed as a vector, must involve a linear combination of q^i and r^i. Since the coefficient of q^i is annihilated by the Q transverse projector, only the coefficient of r^i contributes to eq. (4.16). We can find this contribution by applying a projector which removes the piece proportional to q^i:

$$\begin{aligned} M^{i0}(Q,R) &\equiv r^i M_{T-L}(Q,R) + \text{ Terms proportional to } q^i\,, \\ M_{T-L}(Q,R) &= \frac{1}{p^2 q_\perp^2}(q^2 r^i - q\cdot r q^i) M^{i0}\,, \end{aligned} \tag{4.17}$$

in which $q_\perp$ denotes the component of q perpendicular to p, $q_\perp^2 p^2 \equiv |q\times p|^2 = |q\times r|^2 = |r\times p|^2$.

Now consider the contributions where both propagators are transverse. The function M_{ij} vanishes when contracted against one in-plane and one out-of-plane polarization vector, by parity invariance in the out-of-plane direction. Therefore there are two contributions, one arising from the in-plane projection of M_{ij} and one from the out-of-plane projection of M_{ij}. The out-of-plane projection is

$$M_{T-T,A}(Q,R) = \left(\delta^{ij} - \frac{r^2 q^i q^j + q^2 r^i r^j - q\cdot r q^i r^j - q\cdot r q^j r^i}{p^2 q_\perp^2}\right) M^{ij}\,, \tag{4.18}$$

and the in-plane projection, obtained by dotting M_{ij} against the in-plane polarization operator for each propagator, is

$$M_{T-T,B}(Q,R) = \frac{qr}{p^2 q_\perp^2}\left(r^i - \frac{q\cdot r}{q^2} q^i\right)\left(q^j - \frac{r\cdot q}{r^2} r^j\right) M^{ij}\,. \tag{4.19}$$

Using this procedure we find

$$\begin{aligned} \text{eq. (4.16)} = {} & |M^{00}|^2 G^{00}(Q)G^{00}(R) + 2r^2 q_\perp^2 |M_{T-L}(Q,R)|^2 G^T(Q)G^{00}(R) \\ & + |M_{T-T,A}(Q,R)|^2 G^T(Q)G^T(R) + |M_{T-T,B}(Q,R)|^2 G^T(Q)G^T(R)\,. \end{aligned} \tag{4.20}$$

We have evaluated the scalar functions entering eq. (4.20) in terms of linear combinations of $M^{00}(Q,R)$, 1, and two new functions $L(Q)$ and $L(R)$, with momentum-dependent coefficients (that are real and analytic functions of q^0.) In a condensed notation the result can be written:

$$\text{eq. (4.20)} = \sum_i P_i\, G^{Q_i}(Q) G^{R_i}(R) M_i(Q,R) M_i(Q,R)^*\,, \tag{4.21}$$

$$M_i(Q,R) = X_i M^{00}(Q,R) + Y_{Q_i} L(Q) + Y_{R_i} L(R) + Z_i\,, \tag{4.22}$$

with

$$L(Q) \equiv \int \frac{d\Omega_v}{4\pi} \frac{1}{v\cdot Q^-} \tag{4.23}$$

and $M^{00}(Q,R)$ as defined in eq. (4.6). The sum over i in eq. (4.21) covers the four cases L-L, T-L, T-T,A and T-T,B. The momentum-dependent coefficients X_i, Y_{Q_i}, Y_{R_i} and Z,

Index i	Prefactor P_i	G^{Q_i}	G^{R_i}	X_i
L-L	1	G^{00}	G^{00}	1
T-L	$2/q^2p^2q_\perp^2$	G^T	G^{00}	$-q^0p\cdot q$
T-T,A	1	G^T	G^T	$1-q_0^2/q_\perp^2$
T-T,B	$1/q_\perp^4p^4q^2r^2$	G^T	G^T	$-q_0^2p\cdot qp\cdot r$

Index i	Y_{Q_i}	Y_{R_i}	$Z_i^{(\mathrm{HTL})}$	$Z_i^{(\mathrm{tree})}$
L-L	0	0	0	0
T-L	q^2	$-q\cdot r$	0	$2/q^0m_D^2$
T-T,A	$q^0p\cdot q/p^2q_\perp^2$	$-q^0p\cdot r/p^2q_\perp^2$	0	$-2/m_D^2$
T-T,B	$q^0q^2p\cdot r$	$-q^0r^2p\cdot q$	$p^2q_\perp^2$	$2q\cdot rq_\perp^2p^2/m_D^2$

Table 2: The coefficients in the expansion eq. (4.21). The coefficient Z_i appearing in the text is the sum of its HTL and tree contributions $Z_i^{(\mathrm{HTL})}$ and $Z_i^{(\mathrm{tree})}$, respectively.

as well as the prefactors P_i and choices of propagators, G^{Q_i} and G^{R_i}, are tabulated in table eq. (2). In this table we have separated the contributions to the "constant term" Z coming from the HTL and tree vertices. The various discontinuities of $M_{\mu\nu}$ which enter eq. (4.14) can be obtained from the discontinuities of the basis functions entering eq. (4.22), which are described in detail in appendix A.

4.3.4 Final expressions for diagram (A)

The Wightman self-energy $\Pi^{>\,00}$ enters the heavy quark diffusion coefficient κ through:

$$\kappa_{(A)} = \frac{g^2C_H}{3}\int\frac{d^3p}{(2\pi)^3}\frac{p^2}{(p^2+m_D^2)^2}\Pi_{(A)}^{>\,00}(p)\,. \tag{4.24}$$

Substituting formula eq. (4.14) into this, upon rescaling variables by m_D and scaling out the prefactor from eq. (2.5) in order to obtain the dimensionless contribution to C, we obtain, using the decomposition eq. (4.21) and the results of appendix A:

$$\begin{aligned} C_{(A),\mathrm{main}} = 3\pi\int_p\frac{p^2}{(1+p^2)^2}\int_Q\sum_i P_i \\ \times\begin{cases} \rho^{Q_i}(Q)\rho^{R_i}(-R)\,\big[(\mathrm{Re}\,M_i-\mathrm{Re}\,K_i)^2-(\mathrm{Im}\,K_{Q_i})^2 \\ \qquad -(\mathrm{Im}\,K_{R_i})^2+(\mathrm{Re}\,K_i)^2\big] \\ +4\,\mathrm{Im}\,G^{Q_i}(Q)\rho^{R_i}(R)\,[(\mathrm{Re}\,M_i-\mathrm{Re}\,K_i)\,\mathrm{Im}\,K_{Q_i}+\mathrm{Re}\,K_i\,\mathrm{Im}\,K_{R_i}] \\ +4\rho^{Q_i}(Q)\,\mathrm{Im}\,G^{R_i}(R)\,[(\mathrm{Re}\,M_i-\mathrm{Re}\,K_i)\,\mathrm{Im}\,K_{R_i}+\mathrm{Re}\,K_i\,\mathrm{Im}\,K_{Q_i}] \\ +8\,\mathrm{Im}\,G^{Q_i}(Q)\,\mathrm{Im}\,G^{R_i}(R)\,[(\mathrm{Re}\,M_i-\mathrm{Re}\,K_i)\,\mathrm{Re}\,K_i-\mathrm{Im}\,K_{Q_i}\,\mathrm{Im}\,K_{R_i}]\,, \end{cases} \end{aligned} \tag{4.25}$$

in which:

$$\begin{aligned}
\operatorname{Re} M_i - \operatorname{Re} K_i &\equiv -X_i \frac{\tan^{-1}\left(\frac{p\sqrt{q_\perp^2-q_0^2}}{p\cdot q}\right) + \tan^{-1}\left(\frac{p\sqrt{q_\perp^2-q_0^2}}{p\cdot r}\right) - \frac{\pi}{2}}{p\sqrt{q_\perp^2-q_0^2}} \\
&\quad -Y_{Q_i}\frac{1}{2q}\ln\left(\frac{q+q^0}{q-q^0}\right) - Y_{R_i}\frac{1}{2r}\ln\left(\frac{r-q^0}{r+q^0}\right) + Z_i, \\
\operatorname{Im} K_{Q_i} &\equiv Y_{Q_i}\frac{\pi}{2q}, \\
\operatorname{Im} K_{R_i} &\equiv Y_{R_i}\frac{\pi}{2r}, \\
\operatorname{Re} K_i &\equiv -X_i \frac{\pi}{2p\sqrt{q_\perp^2-q_0^2}},
\end{aligned} \tag{4.26}$$

when $|q^0| < q_\perp$, and:

$$\begin{aligned}
\operatorname{Re} M_i - \operatorname{Re} K_i &\equiv -X_i \frac{\ln\left(\frac{|p\cdot q+\sqrt{q_0^2-q_\perp^2}|}{|p\cdot q-\sqrt{q_0^2-q_\perp^2}|}\frac{|p\cdot r+\sqrt{q_0^2-q_\perp^2}|}{|p\cdot r-\sqrt{q_0^2-q_\perp^2}|}\right)}{2p\sqrt{q_0^2-q_\perp^2}} \\
&\quad -Y_{Q_i}\frac{1}{2q}\ln\left(\frac{|q^0+q|}{|q^0-q|}\right) - Y_{R_i}\frac{1}{2r}\ln\left(\frac{|q^0-r|}{|q^0+r|}\right) + Z_i, \\
\operatorname{Im} K_{Q_i} &\equiv X_i \frac{\pi \operatorname{sgn}(p\cdot q)}{2p\sqrt{q_0^2-q_\perp^2}} + Y_{Q_i}\frac{\pi}{2q}\theta(q^2-q_0^2), \\
\operatorname{Im} K_{R_i} &\equiv -X_i \frac{\pi \operatorname{sgn}(p\cdot r)}{2p\sqrt{q_0^2-q_\perp^2}} + Y_{R_i}\frac{\pi}{2r}\theta(r^2-q_0^2), \\
\operatorname{Re} K_i &\equiv 0,
\end{aligned} \tag{4.27}$$

when $|q^0| > q_\perp$. The arctangents on the first line of eq. (4.26) take values in $[0,\pi]$. The coefficients P_i, X_i, Y_{Q_i}, Y_{R_i} and Z_i, as well as the choices of propagator (transverse or longitudinal), for the different choices of i, are listed in table 2. Expressions for the HTL-resummed retarded propagators G_R and $\rho = G_R - G_A$ are given in eq. (3.4). The integrals depend only on one scale, m_D, which we have scaled out and should be set to 1 whenever it shows up in the formulae. As was discussed earlier, the integrand naturally splits into pole-pole, pole-cut and cut-cut contributions, according to whether the energies of the Q and R propagators lie within the space-like region (the Landau cut) or on the plasmon pole.

The integral eq. (4.25) is (linearly) divergent at large q, due to the transverse-transverse pole-pole contribution involving tree interaction vertices, which duplicates the leading-order gluon-scattering contribution eq. (2.4). To obtain the correct contribution to the coefficient $\tilde{C}^{(QCD)}$ defined below eq. (2.5), this leading-order contribution must be subtracted; this subtraction can be understood as part of a systematic matching procedure like that discussed in section 3. More precisely, one should subtract the contribution to eq. (4.25) which arises from the tree vertices (this corresponds to keeping only the Z_i^{tree} part of Z_i in eq. (4.27), using the bare propagators.

The $|q^0| \approx q_\perp$ region presents some subtleties, that are discussed in greater detail in the next section: due to the square root singularities that appear in the vertex functions (in the terms proportional to X_i, in eq. (4.26)–eq. (4.27), which enter squared in eq. (4.25), the frequency integral is potentially logarithmically divergent in the limit $q^0 \to q_\perp$. In the next section we verify that the divergences cancel out between the lower and upper limits, $|q^0| \to q_\perp^-$ and $|q^0| \to q_\perp^+$, although not individually. As a consequence the integral must be evaluated using a Cauchy principal value prescription near $q^0 = q_\perp$. Actually in the next section we show that in addition to this Cauchy principal value integral there is an additional $\delta(q^0 - q_\perp)$ type of contribution eq. (4.32), giving $C_{(A),q^0=q_\perp} \simeq 0.023333$.

In addition to this, the zero-frequency leftover eq. (4.15) must also be included:

$$\begin{aligned} C_{(A),q^0=0} &= 3\pi \int_p \frac{p}{(1+p^2)^2} \left[\frac{\tan^{-1}(p)}{p} - \frac{1}{1+p^2} \right] \\ &= \frac{3\pi}{32} \simeq 0.294524 \end{aligned} \tag{4.28}$$

The evaluation of eq. (4.25) was performed by numerical integration independently by the two authors. The integrals giving the cut-cut, pole-cut and pole-pole contributions are respectively four, three, and two-dimensional. The independent evaluations used different reparametrizations of the integration variables. For instance, the cut-cut integration can be parameterized in terms of the magnitudes of $\mathbf{q}$ and $\mathbf{r}$, the angle between them, plus one frequency variable, or in terms of p, $p \cdot q$, $q_\perp^2$, and one frequency variable. Both implementations used the Cauchy principal value prescription near $q^0 = q_\perp$ by "folding" the integrals in order that the two individually divergent parts can be added together under the integration sign and a convergent integral be obtained. We found satisfactory convergence in all cases, and obtain $C_{(A),\mathrm{main}} \simeq 0.5918$. Combining with eqs. (4.28) and (4.32), we thus find $C_{(A),\mathrm{Im}} \simeq 0.9097$.

There exist several ways to decompose eq. (4.25) into different contributions. One way, although probably not gauge-fixing independent, is to separate the contributions according to whether they have tree-level or HTL interaction vertices. Doing so, we find that the contributions involving two HTL vertices are all relatively small, and add up to a relatively modest $\simeq +0.14$. There are two large contributions involving two tree interaction vertices, both of which come from the transverse-transverse loop: one is the pole-pole contribution $\simeq -0.52$, which describes the influence of the plasmon dispersion relations on the scatterings, and the other one is the pole-cut contribution $\simeq +0.56$, which describes scattering processes with the radiation or absorption of a soft plasmon. These two contributions happen to nearly cancel against each other, so the net contribution from diagrams with two tree interaction vertices is also relatively modest, $\simeq 0.12$. The remainder of $C_{(A),\mathrm{main}}$ comes from the HTL-tree diagrams, which add up to $\simeq +0.34$, but originate from a large number of terms with different signs. A large contribution comes from the transverse-transverse cut-cut region, giving $\simeq +0.50$, but this is largely cancelled by the transverse-transverse pole-cut region, giving $\simeq -0.33$. Similar cancellations happen between the transverse-longitudinal cut-cut and pole-cut regions, which respectively give $\simeq -0.20$ and $\simeq +0.18$. The remainder of the HTL-tree contributions comes from the transverse-transverse pole-

pole contribution $\simeq +0.30$. We note that the total transverse-transverse pole-pole contribution, which we expect to be gauge invariant on its own (because this diagram is the only place where two soft transverse plasmons can appear) gives about $\simeq -0.20$.

4.3.5 A subtlelty near $q^0 = q_\perp$

We now investigate in more detail the region $|q^0| \simeq q_\perp$ of eq. (4.25). The purpose of this section is to verify that the logarithmic divergences in this expression cancel out between the lower and upper limits, $|q^0| \to q_\perp^-$ and $|q^0| \to q_\perp^+$, so that this expression makes sense as a Cauchy principal value integral. However, we will show that to take such a prescription is not exactly the correct thing to do, but that in addition there is the contribution eq. (4.32).

One procedure for regulating the divergences near $|q^0| = q_\perp$ is to explicitly keep the $i\epsilon$ terms finite in the denominators of the HTL vertex functions M and K eq. (4.6): in the time domain this regulation procedure is analogous to placing an upper bound on the time separation between the external legs of the self-energy diagram. At finite time separation no divergence is found, so that the cancellation we find in this section means that no significant contribution to diagram (A) arises when the time separation between the external legs becomes large (relative to $1/gT$.) Our writing of eq. (4.25) is entirely compatible with this regularization, since this expression follows from eqs. (4.9) and (4.12) by simply decomposing each term into its real and an imaginary part; the Wightman self-energy $\Pi^>$ is always purely real, even when this regulator is used.

All that gets modified at finite $i\epsilon$ are the the explicit expressions for the HTL vertex functions given in eq. (4.26)–(4.27). The only terms we need to keep track of are those involving the function $M^{00}(Q,R)$ and its discontinuities, e.g. the terms multiplying X_i, since all other terms (and propagators) are well behaved in the kinematic region $|q^0| = q_\perp$. Keeping the $i\epsilon$'s finite in the formulae of appendix A, explicit expressions for the singular part of the various combinations of $M^{00}(Q,R)$ and its discontinuities that enter eq. (4.25) can be obtained:

$$
\begin{aligned}
K_Q &\sim \frac{-\pi}{2p}\left[\frac{\theta(-p\cdot q)}{\sqrt{q_\perp^2-(q^0+i\epsilon)^2}}+\frac{\theta(p\cdot q)}{\sqrt{q_\perp^2-(q^0-i\epsilon)^2}}\right],\\
K_R &\sim \frac{-\pi}{2p}\left[\frac{\theta(-p\cdot r)}{\sqrt{q_\perp^2-(q^0-i\epsilon)^2}}+\frac{\theta(p\cdot r)}{\sqrt{q_\perp^2-(q^0+i\epsilon)^2}}\right],\\
\mathrm{Re}\,K &\sim \frac{-\pi}{4p}\left[\frac{1}{\sqrt{q_\perp^2-(q^0+i\epsilon)^2}}+\frac{1}{\sqrt{q_\perp^2-(q^0-i\epsilon)^2}}\right],\\
\mathrm{Re}\,M-\mathrm{Re}\,K &\sim [2\theta(-p\cdot q)+2\theta(-p\cdot r)-1]\,\mathrm{Re}\,K\,.
\end{aligned}
\tag{4.29}
$$

These expressions are valid at both positive and negative q^0, where the value they take is the complex conjugate of their value at positive q^0. Let us first have a look on the bracket from the first line of eq. (4.25), which multiplies $\rho(Q)\rho(R)$. Using the fact that (because $p\cdot r = p^2 - p\cdot q$) it is impossible for both $p\cdot q$ and $p\cdot r$ to be simultaneously negative, one

can see from eq. (4.29) that the singular behavior of $(\mathrm{Re}\, M - \mathrm{Re}\, K)^2$ is always precisely equal to that of $(\mathrm{Re}\, K)^2$. Thus the singular part of this bracket can be written:

$$2(\mathrm{Re}\, K_Q)^2 - (\mathrm{Im}\, K_Q)^2 - (\mathrm{Im}\, K_R)^2 = \mathrm{Re}(K_Q^2 + K_R^2) \tag{4.30}$$

a result which is explicitly well-behaved and given by a Cauchy principal value integration[12] near $|q^0| = q_\perp$. The bracket on the fourth line, multiplying $\mathrm{Im}\, G(Q)\, \mathrm{Im}\, G(R)$, similarly yields a finite Cauchy principal value integral. The cancellation of the divergences between the lower and upper limits can be seen from the explicit expressions for the divergent part of the bracket:

$$\begin{aligned}(\mathrm{Re}\, M - \mathrm{Re}\, K)\, \mathrm{Re}\, K &\sim \frac{\pi^2}{4p^2} \frac{2\theta(-p\cdot q) + 2\theta(-p\cdot r) - 1}{q_\perp^2 - q_0^2} \theta(q_\perp - q^0)\,, \\ -\mathrm{Im}\, K_Q\, \mathrm{Im}\, K_R &\sim \frac{\pi^2}{4p^2} \frac{\mathrm{sgn}\,(p\cdot q)\mathrm{sgn}\,(p\cdot r)}{q_0^2 - q_\perp^2} \theta(q^0 - q_\perp)\,. \end{aligned} \tag{4.31}$$

The two lines are opposite of each other for all values of the momenta, as follows from the fact that $p\cdot q$ and $p\cdot r$ are never negative at the same time.

The brackets on the second and third lines of eq. (4.25) are manifestly finite when $\epsilon = 0$, since the real parts of M and K are only divergent for $|q^0| \to q_\perp^-$, and the imaginary parts of the K's are only divergent for $|q^0| \to q_\perp^+$: products of these terms contain no divergence. However, at finite ϵ the supports of the divergent parts of these terms overlap with each other, on a region of size $\mathcal{O}(\epsilon)$. The contribution from this region remains finite in the $\epsilon \to 0$ limit, giving rise to a $\delta(q^0 - q_\perp)$-type of contribution. It can be extracted by just taking the imaginary part of products of expressions from eq. (4.29), using the formula mentioned in footnote 12; upon rescaling variables by m_D one obtains the dimensionless contribution to C of eq. (2.5):

$$\begin{aligned} C_{(A),q^0=q_\perp} &= 3\pi^4 \int_p \frac{p^2}{(1+p^2)^2} \int_Q \frac{\delta(q^0 - q_\perp)}{p^2 q_\perp} \sum_i P_i\, X_i^2 \\ &\quad \times \left\{ \begin{array}{l} (\theta(-p\cdot q) - \theta(-p\cdot r)) \\ \times \left[\mathrm{Im}\, G^{Q_i}(Q)\rho^{R_i}(R) + \rho^{Q_i}(Q)\, \mathrm{Im}\, G^{R_i}(R)\right] \\ +\theta(p\cdot q)\theta(p\cdot r) \\ \times \left[\mathrm{Im}\, G^{Q_i}(Q)\rho^{R_i}(R) - \rho^{Q_i}(Q)\, \mathrm{Im}\, G^{R_i}(R)\right] \end{array} \right. \\ &\simeq 0.0233326\,, \end{aligned} \tag{4.32}$$

which turns out to be a small contribution, most of which arising from the transverse-transverse contribution (this result was obtained by numerical quadrature).

4.4 The diagram (B)

The diagram (B) represents the expectation value of the correlator eq. (4.2), in which the

[12] This follows from the standard formula $\frac{1}{x - i\epsilon} = \mathcal{P}\frac{1}{x} + i\pi\delta(x)$, which is applicable here since everything it multiplies is smooth as $q^0 \to q_\perp$.

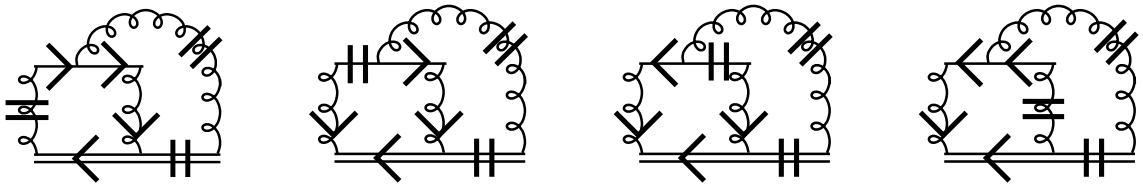

Figure 11: Zoom on the ra structure of the propagators in the HTL diagrams with topology (B), when the zero frequency gauge boson propagator (rightmost one) is cut (rr). These diagrams form a telescopic sum.

heavy quark's Wilson line is expanded to linear order in the A^0 field,

$$\kappa_{(B)} = \frac{C_H g^3}{3d_A} f^{abc} \int_{-\infty}^{\infty} dt \int_0^t dt' \langle \partial^i A^{0\,a}(t)\, A^{0\,b}(t')\, \partial^i A^{0\,c}(0) \rangle, \tag{4.33}$$

$$= \frac{C_H g^3}{3d_A} f^{abc} \int_{Q,R} \frac{2ip\cdot q}{r^0 + i\epsilon} \langle A^{0\,a}(Q)\, A^{0\,b}(R) A^{0\,c}(X=0) \rangle\, 2\pi\delta\left(p^0\right) , \tag{4.34}$$

all fields being Keldysh r fields. The assignment of the momenta in this section is illustrated in figure 7; $P \equiv Q+R$. The fact that one of the fields carries zero frequency is probably best visualized if time translation symmetry is used to move the middle field's time argument to $t' = 0$: restricting the time argument of the leftmost field to $t > 0$ (thus picking up a factor of two), the rightmost field's time argument t'' in the first line of eq. (4.34) is then restricted to the range $-\infty < t'' \leq 0$. However, due to the antisymmetry of the group theory factor, this range can be extended to cover the whole real axis, the contribution from $0 \leq t'' < \infty$ giving zero.

Since there exists no bare interaction vertex with three 0 Lorentz indices, this correlator only receives a contribution from the diagram with an HTL three-point vertex. The dominant diagrams that are allowed by the rules of the ra formalism either involve two cut (rr) gluon propagators and one retarded propagator, with an arr HTL vertex, or one cut propagator and two retarded propagators, and an aar HTL vertex. We find it convenient to organize the resulting diagrams into two classes, according to whether the gluon propagator which carries zero frequency is cut or retarded. When it is cut, one has the HTL diagrams of figure 11, which form a telescopic sum evaluating to:

$$\kappa_{(B),\mathrm{Re}} = \frac{C_H m_D^2 g^4 N_c}{3} \int_{p,Q} \frac{2ip\cdot q}{r^0 + i\epsilon} G^{00}_{rr}(p) \int_v \left\{ \begin{array}{l} -G^{00}_A(Q) \dfrac{1}{v\cdot Q^+} \dfrac{1}{v\cdot R^-} G^{00}_R(R) \\ +G^{00}_R(Q) \dfrac{1}{v\cdot Q^-} \dfrac{1}{v\cdot R^+} G^{00}_A(R). \end{array} \right.$$

$$= -\frac{C_H m_D^2 g^4 N_c}{3} \int_{p,q} G^{00}_{rr}(p) \frac{2p\cdot q}{(q^2+m_D^2)(r^2+m_D^2)} \int_v \frac{1}{v\cdot q^- v\cdot r^+} \,. \tag{4.35}$$

The second line follows from the first by means of contour integration in the complex q^0 plane. The fact that one ends up with an integral involving only zero-frequency propagators is analogous to what happened for the real part of the gluon self-energy diagrams in section 4.2, which we evaluated in terms of the zero Matsubara modes. This is why we called this contribution "$\kappa_{(B),\mathrm{Re}}$". The v integration gives the function $-M^{00}(q,-r)$,

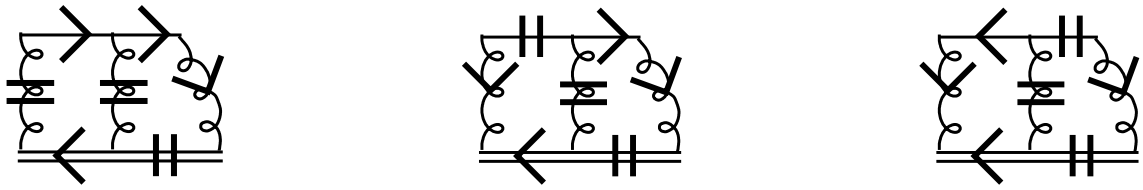

Figure 12: Zoom on the *ra* structure of the propagators in the HTL diagrams with topology (B), when the zero frequency gauge boson propagator (rightmost one) is retarded. Some crossed diagrams are not shown.

which is evaluated in eq. (A.6). Because it is symmetrical under $q \leftrightarrow r$ the factor $2p \cdot q$ can be traded for a p^2. Upon rescaling variables by m_D and scaling out the prefactor $C_H g^4 T^2 m_D/18\pi$ from eq. (2.5), one obtains the dimensionless contribution:

$$\begin{aligned} C_{(B),\mathrm{Re}} &= -6\pi^2 \int_{p,q} \frac{p}{(1+p^2)^2(1+r^2)(1+q^2)} \frac{\pi - \cos^{-1}\left(\frac{q\cdot r}{qr}\right)}{\sqrt{q^2r^2-(q\cdot r)^2}} \\ &\approx -0.0482933\,, \end{aligned} \tag{4.36}$$

in which the branch of the inverse cosine on the first line ranges from 0 to π. The final result was obtained by means of numerical quadrature.

When the zero-frequency gluon propagator in eq. (4.34) is a retarded propagator, one has the HTL diagrams of figure 12, the evaluation of which yields:

$$\kappa_{(B),\mathrm{Im}} = \frac{C_H m_D^2 g^4 N_c}{3} \int_{p,Q} G_A^{00}(p) \left[\frac{iq\cdot p}{r^0+i\epsilon} - \frac{ir\cdot p}{q^0+i\epsilon}\right] \times \begin{cases} G_{rr}^{00}(Q) G_{rr}^{00}(R) q^0 M^{00}(Q,R)^* \\ -T G_R^{00}(Q) G_{rr}^{00}(R) K(Q,P)^* \\ +T G_{rr}^{00}(Q) G_R^{00}(R) K(R,P)^* \\ +2T G_R^{00}(Q) G_{rr}^{00}(R) K(P,Q)\,, \end{cases} \tag{4.37}$$

where we have symmetrized the factors from eq. (4.34) under $(Q \leftrightarrow R)$. This expression bears much similarity to those encountered in section 4.3 for the imaginary part of the self-energy diagram (A). From now on the discussion closely parallels that given there, so we will be brief. Indeed, the first three lines of the brace in eq. (4.37) are very similar to the expressions in eq. (4.9) pertaining to cuts (i) and (ii), except that now there is only one HTL vertex which gets cut. These expressions are also nearly in a form suitable for numerical integration, since they are manifestly supported on the spectral weights of the gluon propagators (they decompose into pole-pole, pole-cut and cut-cut contributions, like eq. (4.25).) However, just like eq. (4.11) from section 4.3, the fourth line of eq. (4.37) poses additional difficulty: its support extends beyond these regions. In section 4.3 this difficulty was dealt with by writing $G_{rr}(R) = (G_R(R) - G_A(R))/(r^0 - i\epsilon)$, then dropping the $G_A(R)$ term using its complex analyticity in the upper-half q^0 plane, and finally using $(Q \leftrightarrow R)$ symmetry to convert $2K(P,Q)$ into the better-behaved combination $(K(P,Q)+K(P,R)) = 2\,\mathrm{Re}\,K(Q,R)$. When one repeats these manipulations here, one first needs to switch the $i\epsilon$ prescription in the $iq\cdot p/(r^0+i\epsilon)$ prefactor in eq. (4.37), in order to make it coherent with the one we wish to introduce. This gives rise to a contribution proportional to $\delta(q^0)$; otherwise the results are very similar.

We note that eq. (4.37) is manifestly real, the contribution from $q^0 < 0$ being the complex conjugate of the contribution from $q^0 > 0$. Taking the real and imaginary parts of each term, as we did in section 4.3.2, the contribution to dimensionless C eq. (2.5) can be written:

$$C_{(B),\mathrm{Im}} = 6\pi \int_{p,q} \frac{p^2}{1+p^2} \left\{ \int \frac{dq^0}{2\pi} \frac{1}{q_0^2} \times \left\{ \begin{array}{l} \rho(Q)\rho(-R)\left[\mathrm{Re}\, M(Q,R) - \mathrm{Re}\, K(Q,P)\right] \\ +2\rho(Q)\,\mathrm{Im}\, G(R)\,\mathrm{Im}\, K(R,P) \\ +2\rho(R)\,\mathrm{Im}\, G(Q)\,\mathrm{Im}\, K(Q,P) \\ +4\left[\mathrm{Im}\, G(Q)\,\mathrm{Im}\, G(R) - |_{q^0=0}\right]\mathrm{Re}\, K(Q,P) \end{array} \right. \right. \\ \left. + \frac{\pi}{2pq_\perp}\left[G_{rr}(q)\,\mathrm{Im}\, G(r) + \mathrm{Im}\, G(q) G_{rr}(r)\right]/T \,. \right. \tag{4.38}$$

$$\simeq \approx -0.07338 \tag{4.39}$$

The fourth line in this expression arises solely from the fourth line of eq. (4.37) and the subtraction "$|_{q^0}$" in it means to subtract $\mathrm{Im}\, G(Q)\,\mathrm{Im}\, G(R)$ evaluated at $q^0 = 0$; this subtraction is convenient because it makes the integrand well-behaved[13] near $q^0 = 0$, and it is justified by the fact that $\int_{-\infty}^{\infty} dq^0 K(P,Q)/(q^0 + i\epsilon)^2 = 0$. A part of the "leftover" from $q^0 = 0$ on the last line of eq. (4.38) arises from the manipulations described in the preceding paragraph, concerning the fourth line of eq. (4.37), and another part of it arises when the real part of the square bracket in eq. (4.37) is taken, since this contains a $\delta(q^0)$ term.

Explicit expressions for the functions $\mathrm{Re}\, M$, $\mathrm{Re}\, K$ and $\mathrm{Im}\, K$ that appear in eq. (4.38) can be obtained by setting $X = 1$ and $Y_Q = Y_R = Z = 0$ in eq. (4.26) and eq. (4.27) of section 4.3.4. We evaluated eq. (4.38) by numerical quadratures; the integration splits into pole-pole, pole-cut and cut-cut contributions (plus the zero-frequency leftover) and their evaluation is very similar to the self-energy diagram (A). There is one important subtlety, though: neither the pole-cut, cut-cut nor $q^0 = 0$ contributions are individually well-defined, as they are all (logarithmically) ultraviolet divergent in the limit of large r, q fixed (taking $r > q$, for definiteness). However their sum is UV convergent; here we skip the explicit verification of this fact. What this implies is that these contributions must be added under the integration sign, e.g. the content of the large brace in eq. (4.38) must be added up before the integration over spatial q and p is performed. The largest part of eq. (4.39) originates from the pole-pole region: thus diagram (B) mostly describes scatterings against longitudinal plasmons (this diagram is an interference term between the Coulomb and Compton channels for longitudinal plasmon scattering.)

4.5 Self-energy (C): imaginary part

The three different diagrams contributing to the cut self-energy diagram of type (C) are shown in figure 13. A direct evaluation of these diagrams would yield:

$$\Pi^{>}_{(b)}{}^{00}(P) = g^2 N_c m_D^2 T \int_Q G^{\mu\nu}_{rr}(Q) \int_v v_\mu v_\nu \left[\frac{2\pi\delta(v\cdot P)}{v\cdot P^- v\cdot (P+Q)^-} \right. \\ \left. + \frac{2\pi\delta(v\cdot(P+Q))}{v\cdot P^- v\cdot P^+} + \frac{2\pi\delta(v\cdot P)}{v\cdot P^+ v\cdot (P+Q)^+} \right]. \tag{4.40}$$

[13] Without this subtraction, the $i\epsilon$ prescription in $1/(q^0 + i\epsilon)^2$ would have had to be explicitly kept.

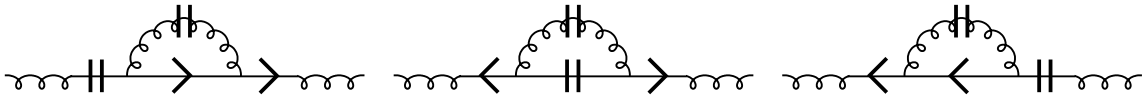

Figure 13: Zoom on the ra structure of the propagators in the HTL diagrams with topology (C).

However, this contains manifestly ill-defined factors such as $\delta(v \cdot P)/v \cdot P^-$. These ill-defined expressions are a typical example of pinch singularities and are due to cuts (i) and (iii) of figure 13, which are attempting to provide self-energy corrections to an on-shell propagator. However, as is well-known, such pinch singularities always cancel out, and in the end one typically obtains expression possessing a "gain-term, loss-term" type of structure characteristic of Boltzmann-like transport equations (see e.g. [37]). In our case the simplest way to regulate the pinch singularities is to use the space-time description of the four-point HTL with two external Keldysh a indices,[14] which is simply given by an adjoint Wilson line along the trajectory of the light particle [27]:

$$\Pi^{>\,00}_{(b)}(P) = -g^2 N_c m_D^2 T \int_v v_\mu v_\nu \int_{-\infty}^{\infty} dt\, e^{-itv\cdot P} \int_0^t dt' \int_0^{t'} dt'' \int_Q e^{-i(t'-t'')v\cdot Q}\, G^{\mu\nu}_{rr}(Q). \tag{4.41}$$

Here t is the time separation between the two endpoints of the Wilson line and the integrand gives the expectation value of a Wilson line in a fluctuating background gauge field, the Wilson line being expanded to second order in the background field and the fluctuations being described by the G_{rr} correlator. Performing the integrations over the time arguments and using the symmetry of $G_{rr}(Q)$ to drop terms which are odd under $Q \to -Q$, one obtains the well-defined integral:

$$\Pi^{>\,00}_{(b)}(P) = g^2 N_c m_D^2 T \int_v v_\mu v_\nu \int_Q G^{\mu\nu}_{rr}(Q)\, 2\pi \frac{\delta(v\cdot(Q+P)) - \delta(v\cdot P)}{(v\cdot Q)^2}\,. \tag{4.42}$$

which has a transparent structure as the sum of a gain term and a loss term.

To evaluate eq. (4.42) we first rotate $\mathbf{q}$ so that its z axis lies aligned with $\mathbf{v}$. The remaining angular integration is over the dot product $u \equiv \mathbf{v}\cdot\mathbf{p}/p$. Although u integration naturally ranges between -1 and 1, by noting that one would obtain zero if it were extended to cover the whole real axis, one can trade it for an integration over $|u| \geq 1$, which we find more convenient for numerical purposes. Upon performing the p integration eq. (4.24), rescaling variables by m_D and factoring out a numerical prefactor, one obtains the contribution to dimensionless C eq. (2.5):

$$\begin{aligned} C_{(C)} &= 6\pi \int_p \frac{-1}{(1+p^2)^2} \int_1^\infty \frac{du}{u^2} \int_q \left[G^{00}_{rr}(up+q_z,q) + (1-q_z^2/q^2) G^T_{rr}(up+q_z,q)\right]/T \\ &\simeq -0.132916 \end{aligned} \tag{4.43}$$

[14] The result we obtain with this regulator agrees with what one would obtain by regulating the pinch singularities by resumming self-energies into the propagators. Indeed, the two regularization methods only differ on frequency scales of order the collisional width (damping rate) $\Gamma \sim g^2 T$, whilst the effects we are looking at take place on the frequency scale gT.

where the correlators G_{rr} are to be evaluated in the soft p^0 approximation $G_{rr}(P) = (G_R(P) - G_A(P))T/q^0$. Although eq. (4.43) can be simplified somewhat (for instance either the u or the p integration, at fixed up, can be done by hand), we had to evaluate it using numerical quadrature. One encounters pole and cut types of contributions in the transverse and longitudinal channels. The result turns out to be almost completely determined by the contribution from the transverse pole, which produces -0.113353 by itself. Thus the important physics described by this diagram is not that of overlapping scattering events, but rather that of tree-level Coulomb scattering processes accompanied with the emission or absorption of a soft transverse gluon (however we do not expect diagram (C) to give a gauge-invariant account of these processes by itself, as the emitted transverse gluon may also be emitted at the exchange gluon, yielding diagrams that are included in (A).)

4.6 The diagram (D)

This diagram involves two insertions of a fluctuating gauge field along the heavy quark's adjoint Wilson line eq. (4.2), and can be written as:

$$\kappa_{(D)} = \frac{-C_H g^4 N_c}{3} \int_{P,Q} \int_{-\infty}^{\infty} dt \int_0^t dt' \int_0^{t'} dt'' \, e^{-itp^0} e^{-i(t'-t'')q^0} p^2 \, G_{rr}^{00}(P) G_{rr}^{00}(Q). \quad (4.44)$$

The structure of this expression is very similar to that of eq. (4.41), met in considering diagram (C), the only difference now being that the Wilson lines lie along the static trajectory of the heavy quark, as opposed to the light-like trajectories of the light plasma particles. Upon performing the time integrations, rescaling variables by m_D and scaling out the numerical prefactor $C_H g^4 T^2 m_D/18\pi$, we obtain the dimensionless contribution:

$$\begin{aligned} C_{(D)} &= 6\pi \int_{p,q} \int \frac{dq^0}{2\pi} p^2 \frac{G_{rr}^{00}(q^0,p) - G_{rr}^{00}(0,p)}{q_0^2} G_{rr}^{00}(q^0,q) \\ &\simeq 0.0675263\,. \end{aligned} \quad (4.45)$$

This was obtained by means of numerical quadrature; the integral splits into pole-pole ($\simeq 0.0474$), pole-cut ($\simeq 0.0261$) and cut-cut ($\simeq 0.0097$) contributions, which respectively require one-, two-, and three-dimensional integrals. In addition there is a contribution coming from the zero-frequency term $G_{rr}^{00}(0,p)$ ($\simeq -0.0156$), whose support in the $q^0 > p$ region needs to be handled separately; these integrals posed no particular difficulty.

This exhausts the diagrams contributing the the momentum diffusion coefficient at next-to-leading order in QCD. Taking the sum of the numbers we obtained we find $\tilde{C} \simeq 1.4946$, with $\tilde{C}$ as in eq. (2.5).

5. $\mathcal{N}$=4 super Yang-Mills

Our setup for $\mathcal{N}$=4 SYM was described in section 2.4. To perform the next-to-leading order calculation we need the appropriate generalization of the force-force correlator and Wilson line appearing in eq. (4.2):

$$\kappa^{(SYM)} = \frac{\lambda^2}{6 d_A} \int_{-\infty}^{\infty} dt \, \langle \partial^i (A^0 + \phi)^a(t) \left[\mathcal{P} e^{\int_0^t dt' [A^0 + \phi, \cdot]} \right]^{ab} \partial^i (A^0 + \phi)^b(0) \rangle \,, \quad (5.1)$$

where ϕ stands for the (canonically normalized) real scalar field of SYM which couples to the nonrelativistic heavy quark. The derivation of this formula is identical to that of eq. (4.2); one must account for the influence of the scalar field on the eikonal propagation of the heavy quark and on the force it feels.[15] In expanding the correlator eq. (5.1) into powers of A^0 and ϕ only the terms with even powers of ϕ have to be kept, since correlators of odd powers of ϕ's vanish by virtue of the global SU(4) R-symmetry of $\mathcal{N}$=4 SYM. The power-counting is the same as for QCD: we need to retain the diagrams with two soft loops. The nonvanishing ones, which we did not previously compute in dealing with QCD, are depicted in figure 14.

Interestingly, these diagrams are significantly easier to evaluate than those of the preceding section, due to the simplicity of HTL amplitudes involving soft scalars: the HTL scalar self-energy reduces to a *momentum-independent* mass shift $m_S^2 = \lambda T^2$, and there exists no HTL effective vertex with external scalars [38]. These features are generic to theories containing scalar fields (with no cubic scalar self-interactions). Physically, the absence of an imaginary part (Landau cut) in the soft scalar two-point function (from which the momentum-independence of the real part of the self-energy follows, by a Kramers-König relation) can be attributed to the spin-suppression of the processes by which soft virtual scalars would be produced by the small-angle scattering of light plasma particles with spin. Indeed these processes, namely Yukawa scattering of fermions and gluon-scalar conversion, both involve a change in the helicity of the light particle. Since the soft virtual scalar carries no polarization tensor, the matrix elements for these processes must be proportional to the deflection angle, which is $\mathcal{O}(g)$ in the HTL limit. Exactly the same mechanism prevents a background scalar field from interfering with the eikonal propagation of relativistic particles with spin, thus suppressing the insertion of external scalar legs onto existing HTL amplitudes.

Perhaps among the most conceptually transparent sources of NLO corrections from soft scalars is that stemming from the imaginary part of the gluon self-energy diagram (A) of figure 14. This diagram produces a negative correction, due to the reduced phase space available for scattering against a massive scalar. Actually, this diagram naturally combines with diagram (D') and with the part of diagram (B) in which the zero-frequency gluon propagator (which is the rightmost propagator) is a retarded propagator: their sum forms a single logical unit, which accounts for the effect of the scalar mass to the tree processes described by the second line of eq. (2.6):

$$\delta\kappa^{(SYM)} = \frac{\lambda^2}{24\pi^3}\int_0^\infty q^3 dq \int_{q/2}^\infty \frac{k^2 dk}{dE_k/dk}\, n_B(E_k)(1+n_B(E_k)) \times \left[\frac{5}{(q^2+m_D^2)^2} + \left(\frac{1}{q^2+m_D^2} - \frac{1}{2E_k^2}\right)^2\right]\Bigg|_{E_k=k}^{E_k=\sqrt{k^2+m_S^2}} . \quad (5.2)$$

Here it is most convenient to trade the k integration for an integration over E_k: the

[15] Had we written the SYM version of eq. (3.1) instead of that of eq. (4.2), the force term would involve the manifestly gauge-covariant combination $(F^{i0} + D^i\phi)$. The spatial gauge fields A^i enter this expression in just such a way as to give total time derivatives which can be dropped, as discussed above eq. (4.2).

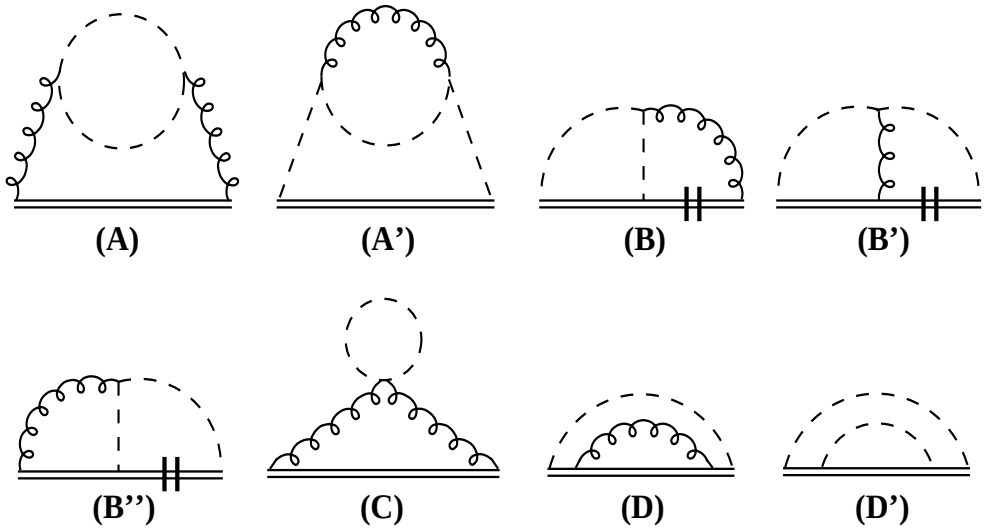

Figure 14: Additional diagrams that contribute to the next-to-leading order momentum diffusion coefficient in $\mathcal{N}$=4 SYM. Not shown, one permutation of (D).

integrand then becomes independent on the functional form of E_k, and the massive and massless results only differ due to the different integration bounds at small E_k. The NLO correction arises from the region $q \sim gT$, in which case the E_k integration ranging from $(q/2)$ to $\sqrt{(q/2)^2 + m_S^2}$ can be done within the approximation $n_B(E_k)(1 + n_B(E_k)) = T^2/E_k^2$. Upon rescaling variables by m_D and factoring out $\lambda^2 T^2 m_D/36\pi$, one obtains the following dimensionless contribution:

$$\begin{aligned}\delta C^{(SYM)} &= -\frac{3}{2\pi^2}\int_0^\infty q^3 dq \left[3\frac{\sqrt{q^2+2}-q}{(q^2+1)^2} - 2\frac{\sqrt{q^2+2}-q}{q\sqrt{q^2+2}(q^2+1)} + \frac{2}{3}\left(\frac{1}{q^3} - \frac{1}{(q^2+2)^{3/2}}\right)\right] \\ &= -\frac{3}{2\pi^2}\left(\frac{-31\sqrt{2}}{6} + \frac{13\pi}{4} - \frac{\cosh^{-1}(\sqrt{2})}{2}\right) \simeq -0.37429 \end{aligned} \tag{5.3}$$

The real part of the zero-frequency self-energy diagram (A) gives zero at NLO, as can be seen using the argument employed in section 4.2: because the interaction vertices are proportional to the loop frequency, in the imaginary time formalism the diagram is saturated by the non-zero Matsubara frequencies, for which no $\mathcal{O}(g)$ corrections arise. The tadpole diagram (C) produces a (negative) momentum-independent shift to m_D^2:

$$\delta m_D^2 = 6\lambda T \int \frac{d^3q}{(2\pi)^3}\left[\frac{1}{q^2+m_S^2} - \frac{1}{q^2}\right] = -\frac{3\sqrt{2}}{4\pi}\lambda T m_D\,, \tag{5.4}$$

which induces a positive shift to C,

$$\delta C^{(SYM)} = 6\pi \int \frac{d^3p}{(2\pi)^3} p^2 G_{rr}^{00}(p) \frac{3\sqrt{2}}{2\pi(1+p^2)} = \frac{9\sqrt{2}}{8\pi} \simeq 0.50643 \tag{5.5}$$

A more or less related virtual contribution arises from the terms in (B) in which the zero-frequency gluon propagator is cut:

$$\delta\kappa^{(SYM)} = \frac{\lambda^2}{6} 2i \int_{p,Q} p^2 G_{rr}(p) \left[G^{(S)}_{rr}(Q) G^{(S)}_{R}(R) + G^{(S)}_{R}(Q) G^{(S)}_{rr}(R) \right] . \tag{5.6}$$

The pattern of propagators in the bracket is the same as usually arises in the calculation of one-loop retarded self-energies, and because the corresponding external momentum P carries zero frequency, one finds that the dominant result at soft p can be expressed in terms of the contribution from the zero Matsubara frequency. This can be derived from eq. (5.6) by writing $G_{rr}(Q) = (G_R(Q) - G_A(Q))T/(q^0 - i\epsilon)$ in the first term, and using analyticity in the upper-half q^0 plane to drop the $G_A(Q)$ contribution, thus turning this term into $G_R(Q)G_R(R)T/(q^0 - i\epsilon)$. Similar manipulations on the second term of the bracket yield $G_R(Q)G_R(R)T/(r^0 - i\epsilon)$, which cancels against the first leaving only a δ-function at $q^0 = 0$. Rescaling variables by $m_{\scriptscriptstyle D}$ one thus obtains the dimensionless contribution:

$$\delta C^{(SYM)} = 12\pi^2 \int_{p,q} \frac{p}{(p^2+1)^2} \frac{1}{(q^2+\frac{1}{2})(r^2+\frac{1}{2})} = \frac{3}{2\pi} \int_0^\infty \frac{p^2\, dp}{(1+p^2)^2} \tan^{-1} \frac{p}{\sqrt{2}} \simeq 0.37044\,. \tag{5.7}$$

Corrections to the real part of the scalar self-energy are irrelevant at NLO, due to the vanishing of the imaginary part of the HTL scalar self-energy. The corrections (A') to the imaginary part of the scalar self-energy naturally combine with diagrams (B'), (B") and (D) to form a single logical unit (in diagrams (B') and (B") the zero-frequency scalar propagator must be a retarded propagator, again because the imaginary part of the HTL scalar self-energy vanishes.) Together they describe the effects of the scalar mass and plasmon dispersion relation on tree-level gluon-scalar scattering, as well as new processes, involving physical longitudinal plasmons in the external states or overlapping scattering events (associated with gluon propagators in the Landau cut.) Processes involving longitudinal gluons also occur in a Compton-like channel, which interferes with the scalar-exchange channel: this is what diagrams (B'), (B") and (D) account for. Using formulae eq. (4.34) and eq. (4.45) these diagrams add up to:

$$\begin{aligned} \delta C^{(SYM)} &= 6\pi \int_{p,Q} G^{(S)}_{rr}(R) \left[4p^2 G^{T}_{rr}(Q) \frac{p^2 - \frac{(p\cdot q)^2}{q^2}}{(p^2+\frac{1}{2})^2} + p^2 G^{00}_{rr}(Q) \left(\frac{q^0}{p^2+\frac{1}{2}} - \frac{1}{q^0} \right)^2 - \frac{q^2}{q_0^2} G^{00}_{rr}(q,0) \right] \\ &\simeq -0.31086\,. \end{aligned} \tag{5.8}$$

The contribution from the transverse gauge field is linearly divergent at large momenta, where it degenerates to the tree-level contribution which was already included in eq. (2.6); this must be subtracted. What we have integrated numerically is the difference between eq. (5.8) and the same expression evaluated with the tree G_{rr} propagators, which is given by a convergent integral. The integral splits into pole-pole and pole-cut contributions, with the largest contribution arising from the transverse gluon pole, which gives $\simeq -0.283$.

This exhausts the list of NLO contributions whose origin is proper to the SYM theory. Taking the sum of eqs. (5.3), (5.5), (5.7) and (5.8) we obtain the next-to-leading order coefficient $\tilde{C}^{(SYM)} = 0.19172$.

Acknowledgments

This work was supported in part by the Natural Sciences and Engineering Research Council of Canada.

A. The functions $M^{00}(Q,R)$ and $L(Q)$

The functions $M^{00}(Q,R)$ and $L(Q)$ have appeared in some form or the other in previous work ([35, 36, 18], to cite a few.) The function $L(Q)$ is familiar from the longitudinal HTL gluon self-energy:

$$\begin{aligned} L(Q) &= \int \frac{d\Omega_v}{4\pi} \frac{1}{v\cdot Q^-} \\ &= \frac{-1}{2q} \ln\left(\frac{q^0+q+i\epsilon}{q^0-q+i\epsilon}\right). \end{aligned} \tag{A.1}$$

The branch of the logarithm is such that this function is real for time-like Q, and acquires a positive imaginary part at space-like Q, the so-called Landau cut.

To understand the analytic structure of $M^{00}(Q,R)$ we find convenient to express it as a sum of two terms,

$$M^{00}(Q,R) = M^{00}(P,Q) + M^{00}(P,R)\,, \tag{A.2}$$

and to analyze those two terms separately. Actually, the splitting of eq. (A.2) as a sum of two terms is precisely how the function $M^{\mu\nu}(Q,R)$ arose in the first place, in the HTL effective vertices of figure 9, so in a sense it is rather natural. In [18] an expression for the (Lorentz-invariant) function $M^{00}(P,Q)$ was obtained by first combining the denominators $1/v\cdot P^-$ and $1/v\cdot Q^-$ by means of standard Feynman parameterization:

$$M^{00}(Q,P) = \int_v \frac{1}{v\cdot P^- v\cdot Q^-} \tag{A.3}$$

$$\begin{aligned} &= \int_0^1 dx \int_v \frac{1}{\left[x\,v\cdot Q + (1-x)v\cdot P - i\epsilon\right]^2} = \int_0^1 dx \frac{-1}{\left(xQ+(1-x)P\right)^2 - i\epsilon q^0} \\ &= \frac{-1}{2\sqrt{-\Delta}} \ln\left(\frac{Q\cdot P+\sqrt{-\Delta}}{Q\cdot P-\sqrt{-\Delta}}\right)\Bigg|_{q_0\equiv q^0+i\epsilon}, \end{aligned} \tag{A.4}$$

where:

$$\Delta = Q^2P^2 - (Q\cdot P)^2. \tag{A.5}$$

Proper care must be given to the $i\epsilon$ prescriptions in eq. (A.4), since we are interested in this function and its discontinuities at physical values of the momenta. The correct procedure follows from noting that, from its definition, the function $M^{00}(Q,P)$ is analytic in the upper half complex q^0 plane. Its integral representation is unambiguous for Q time-like, in which case it has no discontinuity across the real axis, as a function of q^0, with fixed p^0, $\mathbf{p}$ and $\mathbf{q}$. Using a change of variables $\mathbf{v}\to-\mathbf{v}$ in the integral representation eq. (A.3),

one shows that flipping the sign of q^0 in $M^{00}(Q,P)$ is equivalent to complex conjugation. Explicit expressions, when $q^0 \geq 0$, are:

$$M^{00}(Q,P) = \begin{cases} \dfrac{-1}{2p\sqrt{q_0^2 - q_\perp^2}} \left[\ln\left(\dfrac{p\cdot q + p\sqrt{q_0^2 - q_\perp^2}}{-p\cdot q + p\sqrt{q_0^2 - q_\perp^2}} \right) + i\pi \right], & q^0 > q, \\ \dfrac{-1}{2p\sqrt{q_0^2 - q_\perp^2}} \left[\ln\left(\dfrac{p\cdot q + p\sqrt{q_0^2 - q_\perp^2}}{p\cdot q - p\sqrt{q_0^2 - q_\perp^2}} \right) + 2\pi i\,\theta(-p\cdot q) \right], & q_\perp < q^0 < q, \\ \dfrac{-1}{p\sqrt{q_\perp^2 - q_0^2}} \left[\tan^{-1}\left(\dfrac{p\sqrt{q_\perp^2 - q_0^2}}{p\cdot q} \right) \right], & 0 < q^0 < q_\perp, \end{cases} \tag{A.6}$$

where all logarithms are real, and the arctangents range from 0 to π.

The equations eq. (A.6) can be understood from eq. (A.4) as follows. When $q^0 > q$, the magnitude of the square root is automatically larger than $|q\cdot p|$, thus the denominator in the logarithm in eq. (A.4) is negative. Since this denominator has a small negative imaginary part, the logarithm acquires a positive phase $+i\pi$. This choice of branch can be verified from the large q^0 limit, where $M^{00}(Q,R) \to -i\pi/2pq^0$ according to its definition eq. (A.3). When q^0 crosses q (Q becomes spacelike), the square root becomes equal to $|q\cdot p|$, hence either the numerator or the denominator of the logarithm vanishes. Which one vanishes depends on the sign of $q\cdot p$, explaining the appearance of the $\theta(-q\cdot p)$ function in the second case. Finally, when $q^0 < q_\perp$, the square root becomes imaginary and the logarithm goes over to an arctangent.

The function $K^{00}(Q,P)$ is (half) the discontinuity of $M^{00}(Q,P)$ across the real q^0 axis, and can be extracted from the previous results by writing $K(Q,P) = (M(Q,P) + M(-Q,P))/2$:

$$K^{00}(Q,P) = \begin{cases} 0, & q < q^0, \\ \dfrac{i\pi\,\mathrm{sgn}\,(p\cdot q)}{2p\sqrt{q_0^2 - q_\perp^2}}, & q_\perp < q^0 < q, \\ \dfrac{-\pi}{2p\sqrt{q_\perp^2 - q_0^2}}, & 0 < q^0 < q_\perp. \end{cases} \tag{A.7}$$

References

[1] V.A. Rubakov and M.E. Shaposhnikov, *Electroweak baryon number non-conservation in the early universe and in high-energy collisions*, *Usp. Fiz. Nauk.* **166** (1996) 493 [*Phys. Usp.* **39** (1996) 461] [hep-ph/9603208];
A.G. Cohen, D.B. Kaplan and A.E. Nelson, *Progress in electroweak baryogenesis*, *Ann. Rev. Nucl. Part. Sci.* **43** (1993) 27 [hep-ph/9302210].

[2] W. Buchmüller, P. Di Bari and M. Plümacher, *Leptogenesis for pedestrians*, *Ann. Phys. (NY)* **315** (2005) 305 [hep-ph/0401240];

W. Buchmüller, R.D. Peccei and T. Yanagida, *Leptogenesis as the origin of matter*, *Ann. Rev. Nucl. Part. Sci.* **55** (2005) 311 [hep-ph/0502169].

[3] J. Pradler and F.D. Steffen, *Thermal gravitino production and collider tests of leptogenesis*, *Phys. Rev.* **D 75** (2007) 023509 [hep-ph/0608344].

[4] R. Kubo, *Statistical mechanical theory of irreversible processes.* 1. *General theory and simple applications in magnetic and conduction problems*, *J. Phys. Soc. Jap.* **12** (1957) 570.

[5] T. Matsubara, *A new approach to quantum statistical mechanics*, *Prog. Theor. Phys.* **14** (1955) 351.

[6] L.V. Keldysh, *Diagram technique for nonequilibrium processes*, *Zh. Eksp. Teor. Fiz.* **47** (1964) 1515 [*Sov. Phys. JETP* **20** (1965) 1018].

[7] P. Arnold and C.-x. Zhai, *The three loop free energy for high temperature QED and QCD with fermions*, *Phys. Rev.* **D 51** (1995) 1906 [hep-ph/9410360].

[8] E. Braaten and A. Nieto, *On the convergence of perturbative QCD at high temperature*, *Phys. Rev. Lett.* **76** (1996) 1417 [hep-ph/9508406].

[9] K. Kajantie, M. Laine, K. Rummukainen and Y. Schroder, *The pressure of hot QCD up to* $g^6 \ln(1/g)$, *Phys. Rev.* **D 67** (2003) 105008 [hep-ph/0211321].

[10] E. Braaten and R.D. Pisarski, *Soft amplitudes in hot gauge theories: a general analysis*, *Nucl. Phys.* **B 337** (1990) 569.

[11] J.O. Andersen, E. Braaten, E. Petitgirard and M. Strickland, *HTL perturbation theory to two loops*, *Phys. Rev.* **D 66** (2002) 085016 [hep-ph/0205085];
J.O. Andersen, E. Braaten and M. Strickland, *Hard-thermal-loop resummation of the free energy of a hot quark-gluon plasma*, *Phys. Rev.* **D 61** (2000) 074016 [hep-ph/9908323].

[12] J.P. Blaizot, E. Iancu and A. Rebhan, *Approximately self-consistent resummations for the thermodynamics of the quark-gluon plasma. I: entropy and density*, *Phys. Rev.* **D 63** (2001) 065003 [hep-ph/0005003]; *On the apparent convergence of perturbative QCD at high temperature*, *Phys. Rev.* **D 68** (2003) 025011 [hep-ph/0303045].

[13] A. Majumder and C. Gale, *On the imaginary parts and infrared divergences of two-loop vector boson self-energies in thermal QCD*, *Phys. Rev.* **C 65** (2002) 055203 [hep-ph/0111181].

[14] E. Braaten and M.H. Thoma, *Energy loss of a heavy quark in the quark-gluon plasma*, *Phys. Rev.* **D 44** (1991) 2625; *Energy loss of a heavy fermion in a hot plasma*, *Phys. Rev.* **D 44** (1991) 1298.

[15] S. Caron-Huot and G.D. Moore, *Heavy quark diffusion in perturbative QCD at next-to-leading order*, arXiv:0708.4232.

[16] L.D. Landau and E.M. Lifshitz, *Statistical physics*, Addison-Wesley (1969);
S. Ichimaru, *Plasma physics: an introduction to statistical physics of charged particles*, Benjamin-Cummings Publishing Company, California U.S.A. (1986).

[17] H.A. Weldon, *Covariant calculations at finite temperature: the relativistic plasma*, *Phys. Rev.* **D 26** (1982) 1394.

[18] J. Frenkel and J.C. Taylor, *High temperature limit of thermal QCD*, *Nucl. Phys.* **B 334** (1990) 199.

JHEP02(2008)081

[19] G.D. Moore and D. Teaney, *How much do heavy quarks thermalize in a heavy ion collision?*, *Phys. Rev.* **C 71** (2005) 064904 [hep-ph/0412346].

[20] B. Svetitsky, *Diffusion of charmed quarks in the quark-gluon plasma*, *Phys. Rev.* **D 37** (1988) 2484.

[21] C.P. Herzog, A. Karch, P. Kovtun, C. Kozcaz and L.G. Yaffe, *Energy loss of a heavy quark moving through $N = 4$ supersymmetric Yang-Mills plasma*, *JHEP* **07** (2006) 013 [hep-th/0605158].

[22] J. Casalderrey-Solana and D. Teaney, *Heavy quark diffusion in strongly coupled $N = 4$ Yang-Mills*, *Phys. Rev.* **D 74** (2006) 085012 [hep-ph/0605199].

[23] P.M. Chesler and A. Vuorinen, *Heavy flavor diffusion in weakly coupled $N = 4$ super Yang-Mills theory*, *JHEP* **11** (2006) 037 [hep-ph/0607148].

[24] J. Wess and J. Bagger, *Supersymmetry and supergravity*, Princeton University Press, Princeton, U.S.A. (1992).

[25] L.S. Brown, *New use of dimensional continuation illustrated by dE/dx in a plasma*, *Phys. Rev.* **D 62** (2000) 045026 [physics/9911056].

[26] K.C. Chou, Z.B. Su, B.L. Hao and L. Yu, *Equilibrium and nonequilibrium formalisms made unified*, *Phys. Rept.* **118** (1985) 1.

[27] S. Caron-Huot, *Hard thermal loops in the real-time formalism*, arXiv:0710.5726.

[28] J. Kapusta, *Finite temperature field theory*, Cambridge University Press, Cambridge U.K. (1989).

[29] T. Appelquist and R.D. Pisarski, *High-temperature Yang-Mills theories and three-dimensional quantum chromodynamics*, *Phys. Rev.* **D 23** (1981) 2305;
N.P. Landsman, *Limitations to dimensional reduction at high temperature*, *Nucl. Phys.* **B 322** (1989) 498;
K. Farakos, K. Kajantie, K. Rummukainen and M.E. Shaposhnikov, *$3D$ physics and the electroweak phase transition: perturbation theory*, *Nucl. Phys.* **B 425** (1994) 67 [hep-ph/9404201].

[30] H.A. Weldon, *Simple rules for discontinuities in finite temperature field theory*, *Phys. Rev.* **D 28** (1983) 2007.

[31] R.D. Pisarski, *Computing finite temperature loops with ease*, *Nucl. Phys.* **B 309** (1988) 476.

[32] T.S. Evans, *N point finite temperature expectation values at real times*, *Nucl. Phys.* **B 374** (1992) 340.

[33] F. Guerin, *Retarded - advanced N point Green functions in thermal field theories*, *Nucl. Phys.* **B 432** (1994) 281 [hep-ph/9306210].

[34] F. Gelis, *Cutting rules in the real-time formalisms at finite temperature*, *Nucl. Phys.* **B 508** (1997) 483 [hep-ph/9701410].

[35] E. Braaten and R.D. Pisarski, *Calculation of the gluon damping rate in hot QCD*, *Phys. Rev.* **D 42** (1990) 2156.

[36] E. Braaten, R.D. Pisarski and T.C. Yuan, *Production of soft dileptons in the quark-gluon plasma*, *Phys. Rev. Lett.* **64** (1990) 2242.

JHEP02(2008)081

[37] C. Greiner and S. Leupold, *Interpretation and resolution of pinch singularities in non-equilibrium quantum field theory*, *Eur. Phys. J.* **C 8** (1999) 517 [hep-ph/9804239]; *Stochastic interpretation of Kadanoff-Baym equations and their relation to Langevin processes*, *Ann. Phys. (NY)* **270** (1998) 328 [hep-ph/9802312].

[38] E. Braaten and R.D. Pisarski, *Simple effective Lagrangian for hard thermal loops*, *Phys. Rev.* **D 45** (1992) 1827.

JHEP02(2008)081